Geometric and statistical properties induced by separatrix crossings in volume-preserving systems

Anatoly Neishtadt[1], Carles Simó[2] and Alexei Vasiliev[1]

[1] Space Research Institute, Profsoyuznaya 84/32, Moscow 117810, Russia,
aneishta@iki.rssi.ru, valex@iki.rssi.ru

[2] Departament de Matemàtica Aplicada i Anàlisi, Univ. de Barcelona,
Gran Via, 585, Barcelona 08007, Spain, carles@maia.ub.es

June 4, 2002

Abstract

We consider a 3D volume preserving system inside the unit sphere. The system is a small perturbation of an integrable one. Almost all phase trajectories of the integrable system are closed curves. Under an arbitrarily small non-zero perturbation all the interior of the sphere, up to a residue of a small measure, is apparently a domain of chaotic motion. The phenomenon is described as a result of jumps in an adiabatic invariant of the system occurring when a phase trajectory crosses the 2D separatrix of the unperturbed (integrable) system. The dynamical properties can be understood as a consequence of splitting of invariant manifolds under the perturbation. A 2D return map generated by the system possesses strong stretching properties. This makes the dynamics of the system close to hyperbolic. Numerical investigation of the statistical properties of the system demonstrates a good agreement with theoretical predictions made under the assumption that the system has a big ergodic component whose measure tends to the measure of the sphere's interior as the perturbation tends to zero. However, the system is not ergodic, and stable periodic solutions are found, surrounded by stability islands of measure exponentially small with the perturbation.

1 Introduction

There exist several classes of dynamical systems, possessing the following remarkable property. The system differs by a small perturbation from an integrable system. However, at arbitrarily small amplitude of the perturbation the motion apparently becomes chaotic in a large domain in the phase space. The size of this domain does not tend to 0 as the amplitude of the perturbation tends to 0.

This property was observed in numerical experiments, and the reason for this seems in many cases well understood. However, there are no rigorous proofs, and it looks like that currently the dynamical systems theory has no tools for such proofs. Under these circumstances, it seems reasonable to continue numerical studies of the problems, to compare the results with the predictions of the existing non-rigorous theory and to detect the possible non-chaotic motions. In this paper, such a study is carried out for the volume-preserving system

$$\begin{aligned} \dot{x} &= -8xy + \varepsilon z \\ \dot{y} &= 11x^2 + 3y^2 + z^2 - 3 \\ \dot{z} &= 2zy - \varepsilon x. \end{aligned} \tag{1}$$

This system was introduced in [1] as an example of a hydrodynamic flow with chaotic advection ([2]) and in connection with "fast dynamo action" in magneto-hydrodynamics [3], [4]. System (1) satisfies the Stokes equation for a flow of a viscous fluid. The flow can be regarded as a composition of three flows, namely Hill's spherical vortex, a quasi-rigid rotation, and a twist flow.

The unit sphere is invariant under the flow of system (1). For $\varepsilon = 0$ the system is integrable. The numeric simulations seem to show that at arbitrarily small $\varepsilon \neq 0$ the whole interior of the unit sphere, at least up to a small measure, is a domain of chaotic motion (see figure 5). In this paper, we consider the dynamics inside of the unit sphere only. Some results on the dynamics outside of it can be found in [5].

Chaotic dynamics of this system at arbitrarily small $\varepsilon \neq 0$ is apparently produced by jumps of an adiabatic invariant at the separatrix. The theory of jumps of adiabatic invariants at separatrix crossings in Hamiltonian systems with one degree of freedom and the Hamiltonian depending on a slowly varying parameter was developed in [6, 7, 8]; the theory for slow-fast Hamiltonian systems with two degrees of freedom can be found in [9].

The asymptotic formula for the jump in the adiabatic invariant in system (1) was derived in [10]. A similar problem for a different 3D system was considered in [11]. The general situation of separatrix crossing in a volume-preserving 3D system was studied in [5]. The obtained formulae, as it was mentioned in these papers, do not work if a phase trajectory passes too close to the singular points belonging to the separatrix. The formulae in this case for system (1) are obtained in the present paper.

The dynamics in system (1) can be described in terms of a 2D return map. The formulae for the jumps in the adiabatic invariant are used to show that the map has very strong stretching properties everywhere except for a small measure in the domain of its definition. It suggests that the dynamics of the system should be ergodic up to a small measure and makes it necessary to investigate hyperbolic and ergodic properties of the return map numerically. The numerical analysis shows that statistical properties of the system are indeed very close to those of ergodic systems. However, we show that there exist stable periodic solutions. The measure of islands of stability surrounding these solutions is exponentially small with ε.

Stable periodic motions also exist in the region of separatrix crossings in Hamiltonian systems with one degree of freedom and the Hamiltonian depending on a slowly varying parameter under certain additional symmetry conditions [12]. The total measure of the stability islands in this case is a value remaining finite as the perturbation parameter tends to zero. In the system considered in the present paper, the structure of the return map does not allow for existence of islands so large. It looks like that only exponentially small islands can exist in this system.

The outline of the paper is as follows. In Section 2, the basic properties of the system are described. Most of these were established in [10]. We start with the dynamics in the unperturbed system ($\varepsilon = 0$), then the main properties of the perturbed one are considered. The averaging method for this system is described, and the adiabatic invariant is introduced as an integral of the averaged system. The formula for the jump of this adiabatic invariant at the separatrix is obtained. In Section 3, we describe the geometry of the invariant manifolds in the perturbed system. A two-dimensional return map associated with the system is introduced in Section 4. The map is defined in a part of the plane $y = 0$ that is called the fundamental domain. This map adequately describes the dynamics of the system only in the region of the fundamental domain where the formula of Section 2 for the jump in the adiabatic invariant works. The form of the return map in the remaining parts of the fundamental domain is established in Section 5. In Section 6, hyperbolic and ergodic properties of system (1) are studied numerically. The results are compared with theoretical predictions made under the assumption that the system is ergodic. The good agreement suggests that hyperbolicity and ergodicity in the system are violated on a set of a very small measure. Due to existence of stable periodic trajectories, established in the section, the system is definitely not everywhere chaotic, but the size of the domains of ordered motion is negligible and cannot influence observable statistical properties of the system. In the Appendix, proofs and additional details on results presented in Section 2 are given.

2 Basic properties of the system

In this section we briefly put forward the results of [1] and [10]. The proofs can also be found in the Appendix.

2.1 The unperturbed system

The unperturbed ($\varepsilon = 0$) system (1) possesses the following symmetries: $(t, x, y, z) \to (-t, x, -y, z)$, $(t, x, y, z) \to (-t, x, -y, -z)$, $(t, x, y, z) \to (-t, -x, -y, z)$ and $(t, x, y, z) \to (t, -x, y, -z)$. The first symmetry implies that every trajectory that crosses the plane $y = 0$ twice is closed (see [5]). Therefore, in the domain filled by such trajectories, the system has two integrals of motion. The explicit form for these integrals is [1]:

$$I = xz^4, \qquad J = \frac{x^2 + y^2 + z^2 - 1}{z^3}. \tag{2}$$

The intersection of the level surfaces $I = i, J = j$ is an unperturbed phase trajectory $\Gamma_{i,j}$. All the phase trajectories within the unit sphere, except those passing through the poles, are closed (see figure 1 (a)).

The integral J is ill-defined in the plane $z = 0$. In a neighbourhood of this plane, another set of integrals can be used, namely

$$L = |I|^{1/4} \operatorname{sign}(x) \operatorname{sign}(z), \qquad K = |I|^{3/4} J \operatorname{sign}(x) \operatorname{sign}(z). \tag{3}$$

The poles of the unit sphere N and S ($x = z = 0, y = \pm 1$) are singular points with eigenvalues $\lambda_1 = \mp 8$, $\lambda_2 = \pm 6$, $\lambda_3 = \pm 2$. The two-dimensional unstable manifold W_N^u of the point N coincides with the two-dimensional stable manifold W_S^s of the point S. Phase trajectories belonging to these manifolds fill the part of the plane $x = 0$ lying inside the unit sphere. We shall call this surface the separatrix $\mathcal{S}$ of the unperturbed system. Two one-dimensional unstable manifolds of S, namely $h_S^{u,1}, h_S^{u,2}$ coincide with two one-dimensional stable manifolds $(h_N^{s,1}, h_N^{s,2})$ of N correspondingly, forming the curves $h_1 : z = 0, x^2 + y^2 = 1, x < 0$ and $h_2 : z = 0, x^2 + y^2 = 1, x > 0$.

The system also has degenerate singular points that fill the part of the ellipse $\mathcal{E}$: $y = 0,\ 11x^2 + z^2 = 3$ inside the unit circle $y = 0,\ x^2 + z^2 = 1$. These points have one zero eigenvalue and two purely imaginary eigenvalues, equal to $\pm i\,(48 - 20z^2)^{1/2}$. Note, that each unperturbed phase trajectory (except for those passing through the poles) is entangled with this ellipse, and goes upwards through the equatorial plane $y = 0$ outside of the ellipse and downwards inside of it (see figure 1 (a)). This suggests the part of the plane $y = 0$ inside the ellipse as a good section surface to study the dynamics of the system.

Figure 1 (a) displays the invariant sphere, the fixed points N and S and the lines of fixed points from C_1 to C_2 and from C_3 to C_4, as well as the invariant manifolds of N and S . Three orbits, on $x > 0$, $z > 0$, and their projections on the (x, z)-plane show the general behaviour of the closed orbits of the system.

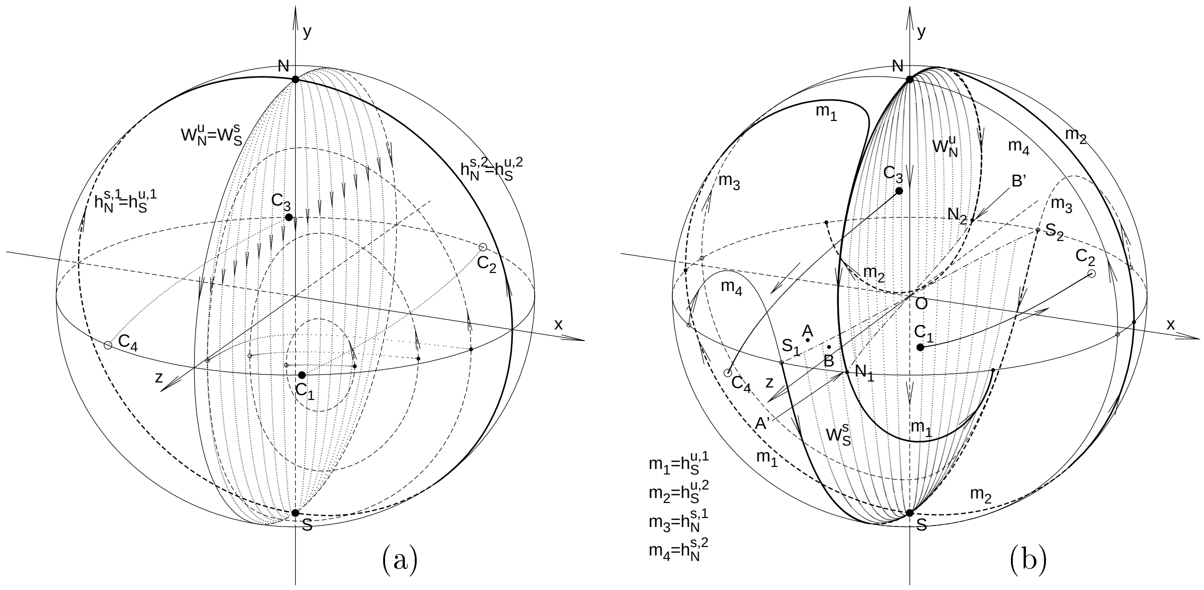

Figure 1: The main characteristics of the flow. (a): the unperturbed system. (b): The perturbed system (the value $\varepsilon = 0.5$ has been used for the illustration).

2.2 The perturbed system

For $\varepsilon \neq 0$ system (1) is no longer integrable. None of the integrals (2) is preserved. However, it retains the following symmetries: $(t, x, y, z) \to (-t, x, -y, -z)$, $(t, x, y, z) \to (-t, -x, -y, z)$ and $(t, x, y, z) \to (t, -x, y, -z)$. In this subsection we describe the main features of the perturbed system, to be analysed in the sequel. We confine our interest to small values of $|\varepsilon|$ and, for definiteness, we shall assume $\varepsilon > 0$.

The fixed points N and S are preserved with the eigenvalues $\lambda_1 = \mp(3 + \sqrt{25 - \varepsilon^2})$, $\lambda_2 = \pm 6$, $\lambda_3 = \pm(\sqrt{25 - \varepsilon^2} - 3)$. The manifolds W_N^u and W_S^s no longer coincide. See figure 1 (b). The separatrix $\mathcal{S}$ is splitted and this is a key phenomenon for the dynamics. In what follows we shall talk about *separatrix crossing* to denote that in the perturbed system the flow crosses the surface $\mathcal{S}$ of the *unperturbed system.* In fact, what produces a dramatic change in the dynamics is the position of the orbit with respect to W^s_S. The two-dimensional manifolds W^u_N and W^s_S have first intersections with $y=0$ on the lines $\mathrm{N}_1\mathrm{O}\mathrm{N}_2$ and $\mathrm{S}_1\mathrm{O}\mathrm{S}_2$, respectively. They define two wedges $\mathrm{N}_1\mathrm{O}\mathrm{S}_1$ (resp. $\mathrm{N}_2\mathrm{O}\mathrm{S}_2$) on $z>0$ (resp. $z<0$), to be studied in section 4. Any orbit inside the sphere, not belonging to the 2D stable and unstable manifolds, will intersect infinitely many times both wedges for forward and backward flow. See figure 2 (a) for a typical path on system (2), where an initial point P, on the wedge with $z>0$, goes to P$'$ on the negative wedge and returns to P$''$, again on the positive wedge.

The one-dimensional invariant manifolds of N and S are also different. They are on the invariant sphere. In figure 1 (b) the branches of these manifolds are denoted as m_j, $j=1,\ldots,4$, according to the coding shown in the figure. The branch m_1 intersects the equator at a point with $x<0$, $z>0$, z small, and then comes close to N. After that it becomes very close to W^u_N, intersecting again $y=0$ extremely close to the point N_1. Finally it spirals tending to C_1. The behaviour of the other branches can be obtained by the symmetries. Note that this pattern occurs for ε not too large. When $\varepsilon>\hat{\varepsilon}$, slightly larger than 1, the part of W^u_N on the surface of the sphere does not intersect the equator. The wedges can still be defined, but they are no longer on the equatorial plane.

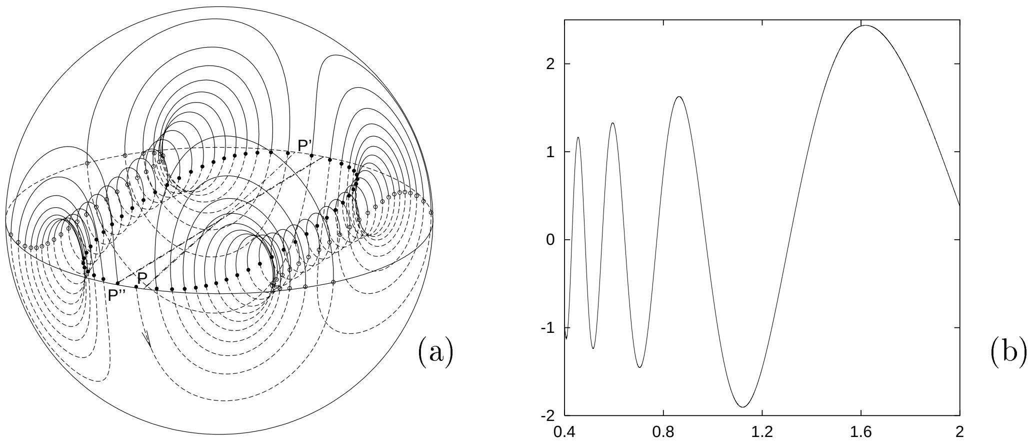

Figure 2: (a): A typical path on the perturbed system. (b): First intersection of $W^u_{C_1}$ with $z=0$ at $(x^*(\varepsilon),y^*(\varepsilon))$. In the plot the function $\exp(11.9/\varepsilon)\,y^*(\varepsilon)$ versus ε is drawn.

The lines of fixed points do not subsist. Only the end points C_j, belonging to the sphere, are fixed points. The coordinates of C_1 are $x=\left((1-\varepsilon^2/16)/5\right)^{1/2}$, $y=\varepsilon/4$, $z=2x$. The corresponding eigenvalues are $3\varepsilon/2$, $-3\varepsilon/4\pm i(32-41\varepsilon^2/16)^{1/2}$. Symmetric coordinates and eigenvalues are found for the other C_j points. Note that the manifolds $W^u_{C_1}$ and $W^s_{C_2}$ (and similar on $x<0$) seem to coincide (here we refer to the branches inside the sphere). In fact the distance between them is very small. The perturbation theory produces exponentially small upper bounds for this distance (see Appendix). We can look numerically at the first intersection of $W^u_{C_1}$ with the plane $z=0$. Let (x^*,y^*) be the coordinates of the intersection. Due to the symmetry the first intersection of $W^s_{C_2}$ with the plane $z=0$ takes place at $(x^*,-y^*)$. The computation of the intersections for a range of ε gives values of the form

$$y^*(\varepsilon)=\exp(-a_1/\varepsilon)\sin(a_2/\varepsilon). \tag{4}$$

Approximate values of a_1, a_2 are 11.9 and 12.2. A plot showing the behaviour of $y^*(\varepsilon)$ is shown in figure 2 (b). In particular, there is a sequence $\varepsilon_k \to 0$, going to zero as $1/k$, for which the manifolds coincide. Between ε_k and ε_{k+1} there are infinitely many values of ε for which $W^u_{C_1}$ reaches the plane $z = 0$ in the region $x < 0$ with $y = 0$. For these values heteroclinic connections from C_1 to C_2, after performing a full revolution around the y axis, occur. In a similar way connections after m revolutions can be found. It is also clear that connections from C_1 to C_4 exist, but we shall not pursue this point.

On the surface of the sphere every point different from N and S and not belonging to the stable manifold of N, goes to a focus, C_1 or C_3, under the forward flow. In a similar way the backward flow leads to C_2 or C_4.

See section 3 for further details on the invariant manifolds of the perturbed system.

2.3 An adiabatic invariant

The averaging method [13] can be used to approximately describe the evolution of the values i, j of the functions I, J in the perturbed $(0 < \varepsilon \ll 1)$ system. The method prescribes to average the rates of changing of i, j in the perturbed motion over the unperturbed motion. Thus we obtain a closed system for the evolution of i, j. It is shown in Appendix (see also [10], [5]) that the averaged system has the form

$$\begin{aligned} \frac{\mathrm{d}i}{\mathrm{d}t} &= \frac{\varepsilon}{T(i,j)} \frac{\partial \Phi(i,j)}{\partial j}, \\ \frac{\mathrm{d}j}{\mathrm{d}t} &= -\frac{\varepsilon}{T(i,j)} \frac{\partial \Phi(i,j)}{\partial i}. \end{aligned} \tag{5}$$

Here $T(i,j)$ is the period of the unperturbed motion along $\Gamma_{i,j}$. The function $\Phi(i,j)$ represents the flux of the perturbation vector $\mathbf{w} = (z, 0, -x)$ across a surface Σ spanning $\Gamma_{i,j}$. Since $\operatorname{div} \mathbf{w} = 0$, this flux is independent of the particular choice of the surface. Thus,

$$\Phi(i,j) = \int_\Sigma (\mathbf{w}, \mathbf{n})\, \mathrm{d}\sigma, \tag{6}$$

where $\mathrm{d}\sigma$ is an area element on Σ and $\mathbf{n}$ is a unit normal vector on Σ directed according to the direction of the angular velocity of the unperturbed motion along $\Gamma_{i,j}$. The function $\Phi(i,j)$ is continuous on the separatrix (at $i = 0$).

Formulae (5) imply that $\Phi(i,j)$ is an integral of the averaged system. The phase portrait of the averaged system (i.e., the portrait of the level lines of function Φ) is shown in figure 3 (a) and (b), on the planes of the variables (j,i) and (k,l), respectively. Last ones are defined as values of the functions K, L in (3). In (a) the separatrix corresponds to the line $i = 0$. The departure of the trajectories to infinity in j is a fictitious singularity associated with the particular choice of variables in the averaged system. Indeed, on the plane (k,l) all the trajectories of the averaged system are closed and 8-shaped due to the fact that on this plane the separatrix is projected onto the origin $k = l = 0$. The motion along trajectories of the averaged system is periodic with period of order ε^{-1}. The direction of motion in the averaged system is shown by arrows. On each period the trajectory crosses the separatrix twice. The bounding trajectories on the plots correspond to motion along the parts of $\mathcal{E}$, connecting points C_1 with C_2 and C_3 with C_4. In figure 3 (c), the intersection of level surfaces of Φ in the (x,y,z)-space with the plane $y = 0$ is shown. While level lines in (a) and (b) are equispaced with respect to the values of Φ, on the (x,z)-plane they are equispaced with respect to the values of Φ^2. The function Φ is equal to zero on the boundary circle and on the line $\mathcal{E}$. The boundary circle corresponds to $j=0$ on the (j,i)-plane and $k=0$ on the (k,l)-plane, respectively. The line $z=0$ on (c) goes to ∞ on (a) and to $l=0$ on (b).

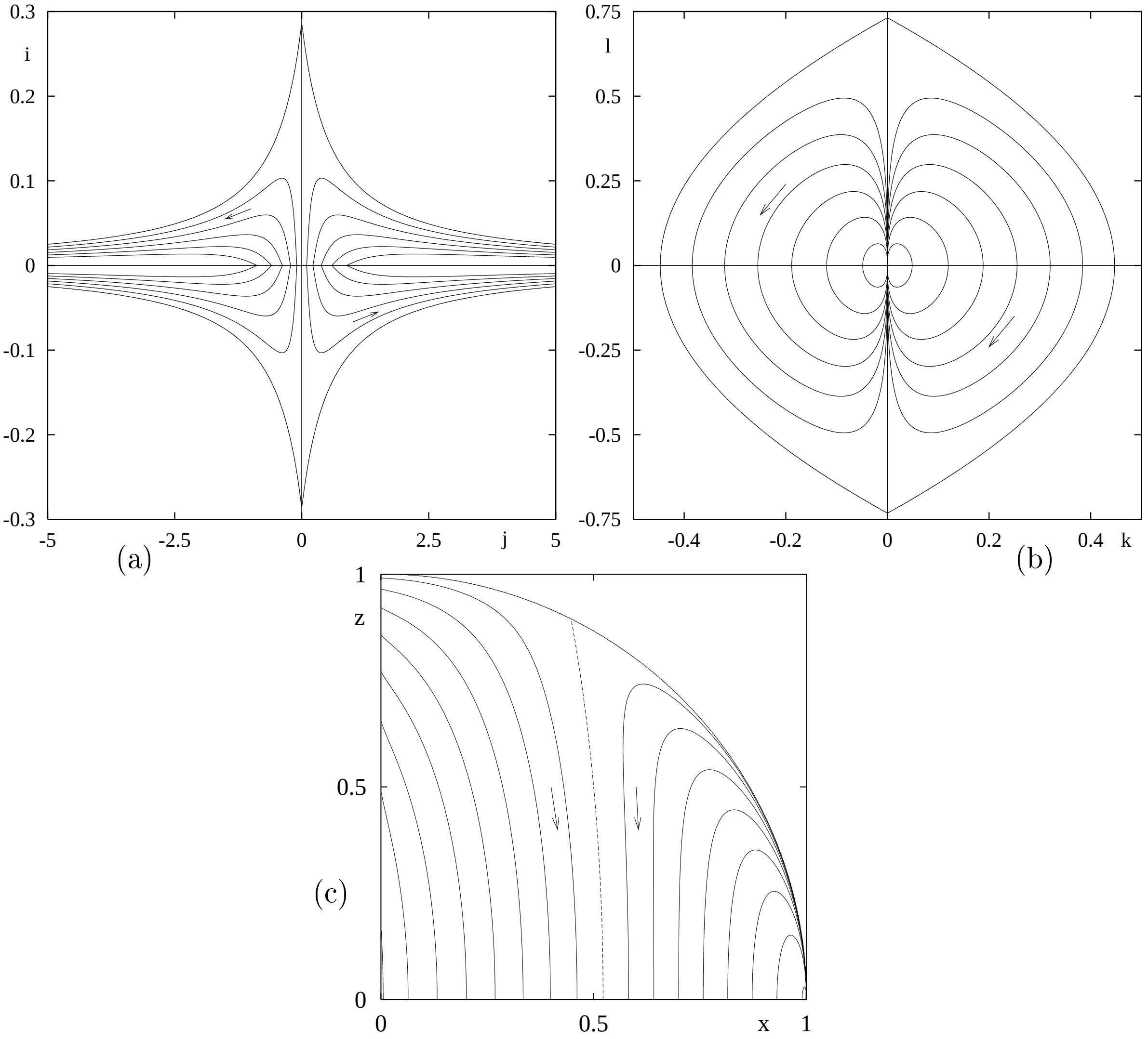

Figure 3: Phase portrait of the averaged system. (a): (j,i) variables. (b): (k,l) variables. (c): Level curves of the function $\Phi(x,y)$ on the plane $y=0$. The curve $\mathcal{E}$ is displayed as a broken line. Only one quarter of the figure is shown.

Note that the level lines on (c) correspond to the approximate paths of the Poincaré iterates for small ε.

Standard assertions about the accuracy of the averaging method (see, for example, [14]) imply that the function Φ is an approximate integral of the motion in the exact system (1), i.e., Φ is an adiabatic invariant.

Along a phase trajectory of (1) far from the separatrix the function Φ undergoes oscillations of order ε over time intervals of order ε^{-1}. Near the separatrix (at $|i|\ll 1$) the accuracy of the averaging method breaks down. The behaviour of Φ along a phase trajectory in a neighbourhood of the separatrix (at $|i|\ll 1$) is described below.

2.4 Asymptotic formula for Φ near the separatrix

At small $i > 0$, the curve $\Gamma_{i,j}$ is close to the contour $\Gamma^+_{0,j}$ consisting of two smooth curves, namely $h_2 : z = 0, x^2 + y^2 = 1, x > 0$ and $s_j = \{J = j\} \cap \mathcal{S}$. Similarly, at $i < 0$ the curve $\Gamma_{i,j}$ is close to $\Gamma^-_{0,j} = s_j \cup h_1$ (see figure 4 (a)).

The adiabatic invariant $\Phi(i, j)$ has a singularity as $i \to 0$. The following asymptotic expansion holds for $|i| \ll 1$ (see Appendix):

$$\Phi(i, j) = \Phi_0(j) - \frac{4}{3} a|j||i|^{3/4} + \mathrm{O}\left(|i|^{5/4}\right), \tag{7}$$

where

$$a = -\frac{3\sqrt{\pi}}{8} \frac{\Gamma(5/8)}{\Gamma(9/8)}.$$

$\Gamma(\cdot)$ denotes the gamma function and $\Phi_0(j)$ is the flux of $\mathbf{w}$ across a surface spanning the contour $\Gamma^\pm_{0,j}$ (the fluxes of $\mathbf{w}$ across surfaces spanning $\Gamma^+_{0,j}$ and $\Gamma^-_{0,j}$ are equal).

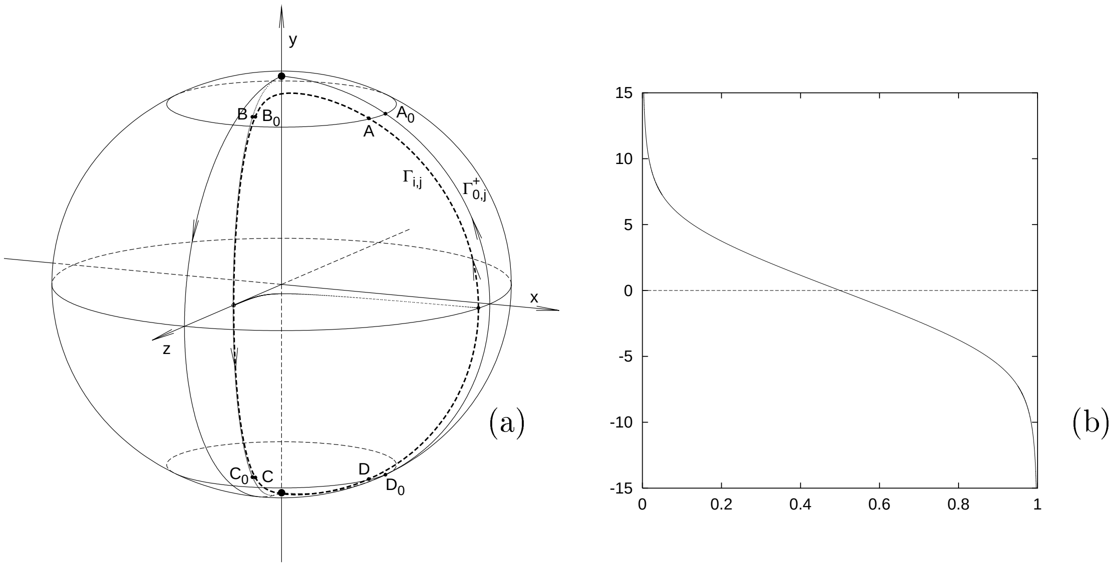

Figure 4: (a): The curve $\Gamma_{i,j}$, approximated by two arcs passing through the poles. (b): Plot of the integral in (10) as a function of ξ.

Let $\Theta = \Theta(j) = \partial\Phi_0/\partial j$. It follows from (5) and (7) that $\varepsilon\Theta(j)$ is the variation of i in the motion along s_j in the averaged system. Thus, one obtains

$$\Theta(j) = \int_{s_j} (\operatorname{grad} I, \mathbf{w})\, \mathrm{d}t. \tag{8}$$

Note, that from the geometrical point of view the function $\varepsilon\Theta(j)$ gives the leading term in the splitting of the invariant manifolds W^u_N and W^s_S in the perturbed system at $y = 0$ (see section 3). The following expression for $\Theta(j)$ holds:

$$\Theta(j) = Z^5 \int_0^1 \frac{v^4 \mathrm{d}v}{\sqrt{(1 - v)(1 + v + v^2 - Z^2 v^2)}}, \tag{9}$$

where $Z = Z(j) \in (-1, 1)$ is the appropriate root of the cubic equation $jz^3 - z^2 + 1 = 0$ (actually, it is the z-coordinate of the point of the intersection of s_j with the equatorial plane).

It follows from (8) and (9) that solutions of the averaged system pass from the domain $i < 0$ to the domain $i > 0$ at $j < 0$ and vice versa at $j > 0$.

2.5 An asymptotic formula for the change in the adiabatic invariant at a separatrix crossing

Consider a segment of a phase trajectory γ of the perturbed system that crosses the separatrix once. Let M_- and M_+ be its initial and final points lying at a distance of order 1 from the separatrix. Figure 2 (a) can be helpful to visualise an arc of a trajectory. Denote by $\Phi_\pm$ the values of $\Phi(i,j)$ at the points $\mathrm{M}_\pm$. Then for $\Delta\Phi = \Phi_+ - \Phi_-$ the following formula holds ([10], see also Appendix):

$$\Delta\Phi = -\varepsilon^{3/4} \left|\Theta_*\right|^{3/4} a|j_*| \frac{4}{\Gamma(1/4)} \int_0^\infty \frac{\sinh\left[(1-2\xi)w^4/2\right]}{\sinh(w^4/2)} \mathrm{d}w + \mathrm{O}\left(\varepsilon\right). \tag{10}$$

(This form of the leading term in $\Delta\Phi$ is obtained from the form in [10] by the change of variable $t \to w^4$.) Here $\Theta_* = \Theta(j_*)$, and j_* is the value of j at the moment of separatrix crossing, calculated in the adiabatic approximation: $\Phi_0(j_*) = \Phi_-$. The value ξ is a function of the initial conditions defined as follows.

Assume for definiteness that γ crosses the separatrix at $z > 0$ $(j < 0)$. The perturbed trajectory γ is a spiral. Denote by M_n the points on γ where $\dot{y} = 0, y > 0$ (the uppermost points on the turns of the spiral). Let us label the points $\{\mathrm{M}_n\}$ as follows. The last of $\{\mathrm{M}_n\}$ before the separatrix crossing has the number 0; $n \le 0$, if $i < 0$; $n > 0$, if $i > 0$; increasing $|n|$ corresponds to receding from the separatrix. We call the turn of the trajectory between the points M_{k-1} and M_k the k-th turn and denote it by γ_k. We denote by $\widetilde{\mathrm{M}}_k$ the point on γ_k where $\dot{y} = 0, y < 0$. We shall use i_k, j_k to represent values of I, J at M_k. By definition $i_0 \le 0$. It is possible to show that $i_0 > -\varepsilon\Theta_0 - C\varepsilon^{7/4}, C = \mathrm{const} > 0, \Theta_0 = \Theta(j_0)$ (because during the turn γ_0 the value i grows approximately by $\varepsilon\Theta_0$, see details in Appendix). Then we define $\xi = -i_0/(\varepsilon\Theta_0)$. Formula (10) holds for

$$C_1\varepsilon^{3/4} \le \xi \le 1 - C_1\varepsilon^{3/4}, \qquad C_1 = \mathrm{const} > 0. \tag{11}$$

The integral in (10) is a function of ξ. Figure 4 (b) shows the plot of this function. It has singularities of the form $\Gamma(1/4)\xi^{-1/4}$ and $\Gamma(1/4)(1-\xi)^{-1/4}$ at the points $\xi = 0$ and $\xi = 1$, respectively.

If condition (11) is not satisfied, the expression (10) for $\Delta\Phi$ is in general not valid. However, if

$$C_2\varepsilon^3 < \xi < C_1\varepsilon^{3/4} \text{ or } 1 - C_1\varepsilon^{3/4} < \xi < 1 - C_2\varepsilon^2, \qquad C_2 = \mathrm{const} > 0 \tag{12}$$

then

$$\Delta\Phi = \varepsilon^{3/4}\mathrm{O}\left(\xi^{-1/4} + (1-\xi)^{-1/4}\right). \tag{13}$$

The behaviour of $\Delta\Phi$ at ξ close to 0 or 1 is discussed in section 5.

3 Invariant manifolds of the perturbed system

The perturbation in (1) splits invariant manifolds of the unperturbed system (see figure 1 (b)). Let $\mathrm{N_1ON_2}$ and $\mathrm{S_1OS_2}$ be the lines of the first intersection of W_N^u and W_S^s with the equatorial plane $y=0$ (the points $\mathrm{N}_{1,2}$, $\mathrm{S}_{1,2}$ lie on the equator; $z>0$ at N_1, S_1 and $z<0$ at N_2, S_2, see figure 1 (b)). The variation in i in the motion along s_j is in the main approximation $\varepsilon\Theta(j)$ (see subsection 2.4). Hence, the lines $\mathrm{N}_1\mathrm{ON}_2$ and $\mathrm{S}_1\mathrm{OS}_2$ are given in the main approximation by the relations $i=\pm\frac{\varepsilon}{2}\Theta(j)$, the plus corresponding to $\mathrm{N}_1\mathrm{ON}_2$, and the minus to $\mathrm{S}_1\mathrm{OS}_2$. Taking into account the expressions (2), (9) for i, j, Θ , we find the equations for these lines:

$$x=\pm\frac{\varepsilon z}{2}\int_0^1\frac{v^4\mathrm{d}v}{\sqrt{(1-v)(1+v+v^2-z^2v^2)}}. \tag{14}$$

Calculating an asymptotic expansion at small z of the integral in (14), one obtains:

$$x=\pm\varepsilon z\frac{16}{21}\frac{\pi^2}{(\Gamma(1/3))^3 2^{2/3}}\approx\pm 0.246\varepsilon z. \tag{15}$$

The manifolds W_N^u and W_S^s intersect along the invariant straight line $x=z=0$. Expression (15) implies that this intersection is transversal, and the angle between W_N^u and W_S^s at $y=0$ is approximately 0.49ε.

The perturbation also splits the invariant manifolds $h_S^{u,1}, h_N^{s,1}$ and $h_S^{u,2}, h_N^{s,2}$. The splitted manifolds stay on the surface of the unit sphere. The points of the first intersections of $h_S^{u,1}, h_S^{u,2}, h_N^{s,1}, h_N^{s,2}$ with the equatorial plane can be found as follows. The variation of $l=|x|^{1/4}z\,\mathrm{sign}(x)\,\mathrm{sign}(z)$ in the motion along $h_{1,2}$ is, in the main approximation,

$$\delta_{1,2}l=\int_{h_{1,2}}(\mathrm{grad}\,L,\mathbf{w})\mathrm{d}t. \tag{16}$$

At the points of first intersection of these four manifolds with the equator one has $x=\pm 1$ in the main approximation. Therefore at these points $z=\pm\delta_{1,2}l/2$. Calculating the integral one obtains:

$$z=\pm\frac{\varepsilon}{2}\int_{h_2}x^{5/4}\mathrm{d}t=\pm\varepsilon\frac{\sqrt{\pi}}{16}\frac{\Gamma(5/8)}{\Gamma(9/8)}=\mp\varepsilon a/6, \tag{17}$$

with $z<0$ for $h_N^{s,1}$ and $h_S^{u,2}$, and $z>0$ for $h_N^{s,2}$ and $h_S^{u,1}$. Thus the splitting is of order ε.

The perturbation also destroys the ellipse $\mathcal{E}$ of degenerate stationary points in the equatorial plane. Only the points $\mathrm{C}_n, n=1,\dots,4$ on the surface of the sphere survive, as mentioned in subsection 2.2, where their positions and eigenvalues were given. They shift from the equatorial plane at a distance of order ε. As it follows from general results of [15], the one-dimensional invariant manifolds of these points are splitted by a value $\mathrm{O}(\exp(-\mathrm{const}/\varepsilon))$. See subsection 2.2 for the experimental evidence on this behaviour. This exponentially small splitting will play an essential role in the problem of the existence of stability islands in the system (i.e., 2D invariant tori of (1); see subsection 6.6.) Furthermore, it makes the problem of constructing a suitable surface of section more difficult, which influences the algorithms for the numerics.

4 The return map

Consider two open domains $\mathcal{D}_1$ and $\mathcal{D}_2$ in the $y=0$ plane. The domains have the form of wedges; the domain $\mathcal{D}_1$ is bounded by the curves ON_1, OS_1, $\mathrm{N}_1\mathrm{S}_1$, and the domain $\mathcal{D}_2$ is bounded by the curves ON_2, OS_2, $\mathrm{N}_2\mathrm{S}_2$. These domains were already mentioned in 2.2.

A typical phase trajectory γ crosses these domains on the turns that cross the separatrix. A phase point that starts the motion in $\mathcal{D}_1$ will, in general, arrive to $\mathcal{D}_2$ after $\mathrm{O}(1/\varepsilon)$ turns of the trajectory (except for the points starting their motion at a distance $\preceq \varepsilon^4$ from the line OS_1, see details in the following section). Thus, the map $\mu\colon \mathcal{D}_1 \to \mathcal{D}_2$ is defined. Similarly, one can define the map $\nu\colon \mathcal{D}_2 \to \mathcal{D}_1$ and the return map $\nu\mu\colon \mathcal{D}_1 \to \mathcal{D}_1$. The properties of this map control the dynamical properties of the system.

Denote as $\mathcal{P}$ the transformation $x \to -x, z \to -z$. As the system (1) is invariant with respect to $\mathcal{P}$, we have $\nu = \mathcal{P}\mu\mathcal{P}$ and, therefore, $\nu\mu = \mathcal{P}\mu\mathcal{P}\mu = (\mathcal{P}\mu)^2$. Hence, it is sufficient to study properties of the map $\mathcal{P}\mu$: $\mathcal{D}_1 \to \mathcal{D}_1$, to be also denoted as return map. The figure 5 shows an example of iterations in $\mathcal{D}_1$ under the return map. The value $\varepsilon = 0.1$ has been used. The initial conditions are $x = 0.3$, $y = 0$, $z = 0$ and the number of iterations is 10^5. It seems that the iterations fill the whole wedge in a quite uniform way.

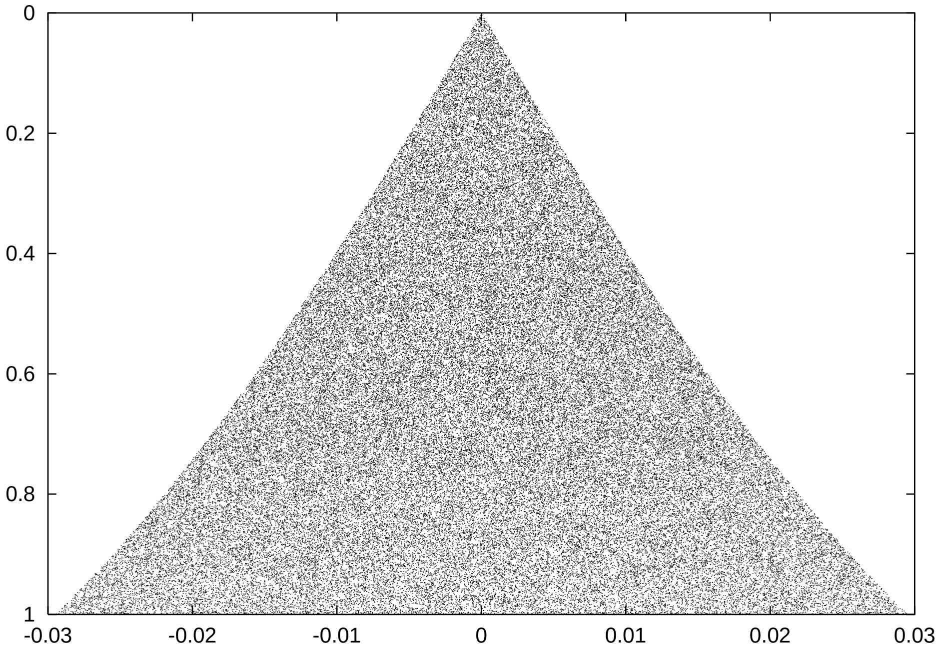

Figure 5: Iterations of the return map $\mathcal{P}\mu$ giving evidence of the chaotic behaviour. The z-axis is directed downwards. See the text for the data used.

As the system is volume-preserving, the map $\mathcal{P}\mu$ preserves the phase flux through an element of the equatorial plane. Therefore, the return map has the invariant measure $\mathrm{d}m = (3 - 11x^2 - z^2)\mathrm{d}x\,\mathrm{d}z \approx (3 - z^2)\mathrm{d}x\,\mathrm{d}z$ (because $x = \mathrm{O}(\varepsilon)$ in $\mathcal{D}_1$).

As coordinates in $\mathcal{D}_1$ one can use the values $\Phi_0(j), \eta$, the latter defined as follows. Denote as $i_{N,S}(j, \varepsilon)$ the values of I at the points of intersection of the line $J = j = \mathrm{const}$ with ON_1 and OS_1; $i_{N,S}(j, \varepsilon) = \pm\frac{\varepsilon}{2}\Theta(j) + \mathrm{O}(\varepsilon^3)$. Let $\Delta i(j, \varepsilon) = i_N(j, \varepsilon) - i_S(j, \varepsilon) = \varepsilon\Theta(j) + \mathrm{O}(\varepsilon^3)$. Introduce $\eta = (i_N(j, \varepsilon) - i)/\Delta i(j, \varepsilon)$. The value of η ranges from 0 to 1 along a line $J = \mathrm{const}$. In terms of Φ_0, η the invariant measure is $\varepsilon^{-1}\mathrm{d}m = (1 + \mathrm{O}(\varepsilon^2))\,\mathrm{d}\Phi_0\mathrm{d}\eta$. (We have used here that $\mathrm{d}m = \mathrm{d}i\,\mathrm{d}j$ and the relation $\Theta(j) = \partial\Phi_0/\partial j$).

For points of the fundamental domain not close to its boundary ($j \sim 1, \eta > C\varepsilon^{3/4}, 1 - \eta > C\varepsilon^{3/4}, C = \mathrm{const} > 0$), one can write approximate formulas for the return map. In these formulas we retain only the main terms. Identify in the main approximation η and ξ. It is convenient to use instead of Φ_0 the variable Ψ which is the value of Φ at the point where the trajectory crosses the plane $z = 0$ between arrival to $\mathcal{D}_1$ and the previous separatrix crossing. Generally, this point lies at $\sim 1/\varepsilon$ turns before arrival to $\mathcal{D}_1$ and $\sim 1/\varepsilon$ turns after the previous separatrix crossing. Then in the main approximation the map $\mathcal{P}\mu$ has the form

$$\begin{aligned} \Psi' &= \Psi + \varepsilon^{3/4} h(\Psi, \eta), \\ \eta' &= \left\{ \eta + \tfrac{1}{\varepsilon}\Omega(\Psi') + q(\Psi', \varepsilon) + \varepsilon^{3/4} p(\Psi', \eta, \varepsilon) \right\}. \end{aligned} \tag{18}$$

Here h is the main term in the right hand side of (10) (one should replace ξ by η and express j_* in terms of Ψ according to the equation $\Phi_0(j_*) = \Psi$). The function Ω is given by the formula

$$\Omega(\Psi) = \frac{1}{2\pi} \int_0^{\tau_*(\Psi)} \omega(I(\Psi, \tau), J(\Psi, \tau)) \mathrm{d}\tau, \tag{19}$$

where $\omega(I, J)$ is the frequency of the unperturbed motion, $(I(\Psi, \tau), J(\Psi, \tau)), \tau = \varepsilon t$, is the motion in the averaged system satisfying $\Phi(I, J) = \Psi$. At the moments 0 and τ_* the trajectory of the averaged system crosses the separatrix. Hence τ_* is a half period of the motion along this trajectory. Functions p, q together with their derivatives are $\mathrm{O}(1)$. The symbol $\{\cdot\}$ denotes the fractional part.

In the map (18), a small change $\delta\eta$ in the value of η produces, in the linear approximation, the change $\delta\eta' = A\delta\eta$ in the value of η'. The stretching coefficient A is given, in the leading approximation, by the formula

$$A = \frac{1}{\varepsilon^{1/4}} \frac{\mathrm{d}\Omega}{\mathrm{d}\Psi} \frac{\partial h}{\partial \eta}. \tag{20}$$

One can check, by numeric investigation, that $\partial\Omega/\partial\Psi \neq 0$, at least if Ψ is not exponentially close to 0 (see the end of this section). It follows from (10) that inside $\mathcal{D}_1$ $\partial h/\partial\eta \neq 0$. Therefore, in the region under consideration at small ε the return map has the strong stretching property: $|\delta\eta'| \sim \varepsilon^{-1/4}|\delta\eta| \gg |\delta\eta|$. As a result, a set of initial points arbitrarily distributed in η is generally redistributed uniformly in this variable in one iteration of the return map. Therefore, one should consider η as a random variable uniformly distributed on $(0, 1)$.

Note that according to (10), $\partial h/\partial\eta$ is proportional to $|j_*|$. Hence, close to the surface of the sphere, this value can be arbitrarily small. However, the stretching coefficient A can still be large in this case. Indeed, a phase trajectory that crosses $\mathcal{D}_1$ close to the surface of the sphere passes, on its way to $\mathcal{D}_2$, close to the saddle-foci C_1, C_2 of the system. Therefore, in this case $\tau_*(\Psi)$ can be estimated as $\tau_*(\Psi) \sim -\ln|\Psi|$ and $\Omega(\Psi) \sim -\ln|\Psi|$. From definition of $\Theta(j)$ one has $j_* \approx \Psi/\Theta(0)$. Combining these expressions, one finds from (20) that as $\Psi \to 0$, $A \to C\varepsilon^{-1/4}$, where C is a constant.

This reasoning, however, does not take into account the splitting of the manifolds $W^u_{C_1}$ and $W^S_{C_2}$. It fails at $|\Psi| < |\Psi^*|$, where $|\Psi^*|$ is exponentially small in ε and corresponds to the point $(x^*, y^*, 0)$ where the one-dimensional invariant manifold of C_1 crosses the plane $z = 0$ (see Section 2.2). In this extremely narrow region, $\mathrm{d}\Omega/\mathrm{d}\Psi$ is bounded, and the coefficient A can turn to zero. As we shall see in Section 6.6, in this region islands of stability exist.

Strong stretching in η is an indication of chaotic behaviour. However, one cannot make conclusions about global hyperbolicity of the map, because stretching decreases at exponentially small magnitudes of Ψ. Besides, formula (10) is not valid for ξ (and hence

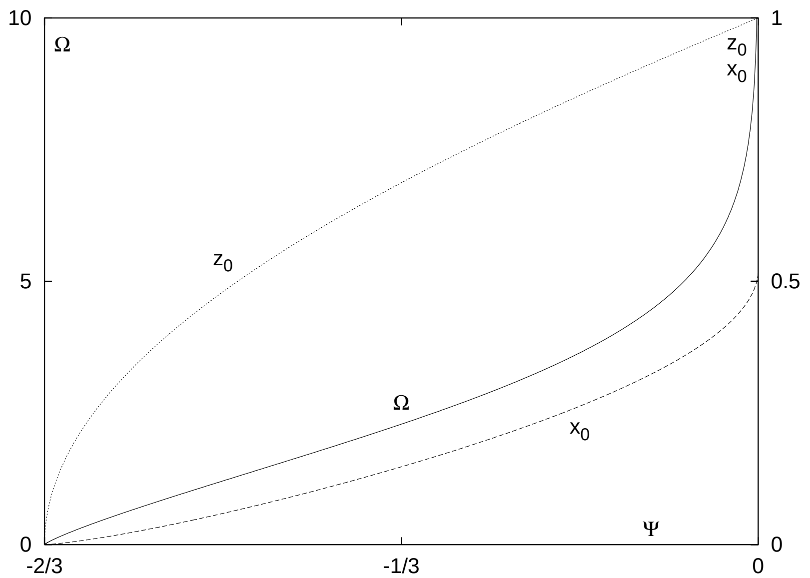

Figure 6: A plot of Ω as a function of Ψ (solid line). For completeness the values of x_0 (broken line) and z_0 (dotted line) as functions of Ψ are also given. They correspond to the values of x when $z = 0$ and z when $x = 0$, respectively, on the integral curve $\Phi = \Psi$ of the averaged system. Compare with figure 3 (c).

for η) close to the endpoints of the interval $(0, 1)$. Properties of the return map in these latter domains are discussed in the next section.

The figure 6 supports numerically the assertion about the increasing character of Ω. The value given by (19) tends to ∞ when $|\Psi|$ tends to 0. The value $\varepsilon^{-1}\Omega(\Psi)$ predicts the number of "revolutions" of the phase trajectory between two consecutive separatrix crossings. These values have been checked against the observed number of revolutions, $\mathrm{NR}_{\mathrm{obs}}(\varepsilon)$ for values of $\varepsilon = 10^{-k}$, $k = 3, 4, 5, 6$ and different initial points (typically starting with $x = \varepsilon$, $z = 10^{-2}j$, $j = 1, \ldots, 99$). It is observed that the difference $\mathrm{NR}_{\mathrm{obs}}(\varepsilon) - \varepsilon^{-1}\Omega$ is essentially independent of ε in agreement with (19). Note, however, that for Ψ sufficiently close to 0 the predictions should fail because of the role played by the invariant manifolds of the C_j points.

Details on the computation of the integral in (19) are given at the Appendix.

5 Properties of the return map near the boundary of the fundamental domain

It was mentioned in section 2 that formula (10) for the change in the adiabatic invariant due to separatrix crossing is not valid if ξ is close enough to the endpoints of the interval $(0, 1)$. In particular, according to this formula, the magnitude of $\Delta\Phi$ tends to infinity as $\xi \to 0$ or $\xi \to 1$ while actual values of $\Phi(i, j)$ are bounded by 0 at the surface of the unit sphere and $-2/3$ at the diameter that connects the poles of the sphere. Therefore, the approximate formula for the return map (18) does not work near the boundary of the fundamental domain at η close to 0 or to 1.

In this section, we derive the asymptotic formula for the change in the adiabatic invariant due to separatrix crossing for η close to 0 or 1. We make rough calculations taking into account only main terms in all expressions. For definiteness, we consider a separatrix crossing in the domain $z > 0$. At the separatrix the x-coordinate changes its sign: $x < 0$ before the crossing, and $x > 0$ after the crossing.

Formula (10) does not work at ξ close to 0 or to 1 because of two reasons. First, in this formula, there should be η instead of ξ, and the replacement of η by ξ gives big relative errors for $\xi < C\varepsilon^3$ and for $1-\xi < C\varepsilon^3$. This is corrected just by putting η instead of ξ in (10). Second, at $\eta < C\varepsilon^3$ and $1-\eta < \varepsilon^3$, big changes of j occur along the trajectory. Hence, the assumptions made in the derivation of (10) are invalid. Indeed, in the derivation of (10) it is supposed that changes in j are small.

The big changes in j occur either on the turn γ_0 (corresponding to $\eta < C\varepsilon^3$ and passage close to the pole N at the end of γ_0 just before the separatrix crossing) or on the turn γ_1 (corresponding to $1-\eta < C\varepsilon^3$ and passage close to the pole S right after the separatrix crossing). These two cases are represented in figure 1 (b) by points A and B and their images A$'$ and B$'$, located, in the wedges, close to N_1 and N_2, respectively. Let us consider the motion in these cases in more detail.

5.1 Properties of the return map at $1-\eta \preceq \varepsilon^3$.

Consider a separatrix crossing at $z > 0$. At the point M_0 let the values of I, J be: $i_0 = -\varepsilon\Theta_0 + \varepsilon\Theta_0(1-\eta)$, j_0. Then at the lower-most point $\widetilde{\mathrm{M}}_1$ of the turn γ_1 we have $\tilde{i}_1 = \varepsilon\Theta_0(1-\eta)$, $\tilde{j}_1 = j_0$, and hence $\tilde{l}_1 = (\varepsilon\Theta_0(1-\eta))^{1/4}$, $\tilde{k}_1 = (\varepsilon\Theta_0(1-\eta))^{3/4}j_0$. The variation in l along the segment $\widetilde{\mathrm{M}}_1\mathrm{M}_1$ of γ_1 is $\delta_2 l = \varepsilon a/3 < 0$ (see (16), (17)). Therefore, if $l_1 = \tilde{l}_1 + \delta_2 l$ is less than zero, i.e. if

$$1-\eta < \frac{\varepsilon^3}{\Theta_0}\left[-\frac{a}{3}\right]^4, \tag{21}$$

the perturbed trajectory γ crosses the plane $z=0$ between the points $\widetilde{\mathrm{M}}_1$ and M_1. This means that right after M_1 this trajectory hits the domain $\mathcal{D}_2$.

The variation in k along $\widetilde{\mathrm{M}}_1\mathrm{M}_1$ is zero in the main approximation. Therefore, if (21) is satisfied, the value of k at the point where the turn γ_1 crosses the plane $z=0$, is $k = (\varepsilon\Theta_0(1-\eta))^{3/4}j_0$. To find the corresponding value of Φ (which equals Ψ' in this case), consider an unperturbed trajectory belonging to the semi-plane $z=0, x>0$. The integral L is zero on this trajectory. Let $|k| = |x^{3/4}(x^2+y^2-1)| \ll 1$ on it. The value of the adiabatic invariant on this trajectory is:

$$\Phi(k) = -\frac{1}{2}\int_{x_{min}}^{x_{max}} \frac{2x^3+\frac{3}{4}x^{1/4}k}{\left(1-x^2+kx^{-3/4}\right)^{1/2}}\mathrm{d}x = -\frac{2}{3}+\frac{\sqrt{\pi}}{2}\frac{\Gamma(5/8)}{\Gamma(9/8)}|k| = -\frac{2}{3}-\frac{4}{3}a|k|. \tag{22}$$

Therefore,

$$\Phi(\eta) = -\frac{2}{3}-\frac{4}{3}a|j_0|(\varepsilon\Theta_0)^{3/4}(1-\eta)^{3/4}. \tag{23}$$

Changing the notations, we obtain:

$$\Psi' = -\frac{2}{3}-\frac{4}{3}a|j_0(\Psi)|(\varepsilon\Theta_0(\Psi))^{3/4}(1-\eta)^{3/4}. \tag{24}$$

To find the expression of η' via η, calculate values of i, j at the point M_1. Note that $k_1 = \tilde{k}_1$. Hence, one obtains:

$$i_1 \quad = \quad \left[(1-\eta)^{1/4}(\varepsilon\Theta_0)^{1/4}+\varepsilon a/3\right]^4,$$

$$j_1 = j_0 \left[1 + \varepsilon \frac{a}{3}(1-\eta)^{-1/4}(\varepsilon\Theta_0)^{-1/4}\right]^{-3}. \quad (25)$$

Right after M_1, the trajectory γ crosses the separatrix at $z < 0$. This crossing is characterized by ξ'. Hence,

$$\xi' = \frac{i_1}{\varepsilon\Theta(j_1)} = \frac{1}{\varepsilon\Theta(j_1)} \left[(\varepsilon\Theta_0)^{1/4}(1-\eta)^{1/4} + \varepsilon a/3\right]^4. \quad (26)$$

Therefore,

$$\eta' = \frac{1}{\varepsilon\Theta(\Psi')} \left[(\varepsilon\Theta_0)^{1/4}(1-\eta)^{1/4} + \varepsilon a/3\right]^4. \quad (27)$$

Expressions (24) and (27) give the return map for $1-\eta < \varepsilon^3\Theta_0^{-1}(a/3)^4$. We do not write the map in the range $(1-\eta) \sim \varepsilon^{-3}$, $1-\eta > \varepsilon^3\Theta_0^{-1}(a/3)^4$, because the expressions are complicated and difficult to interpret. Besides, they are not necessary for the following consideration.

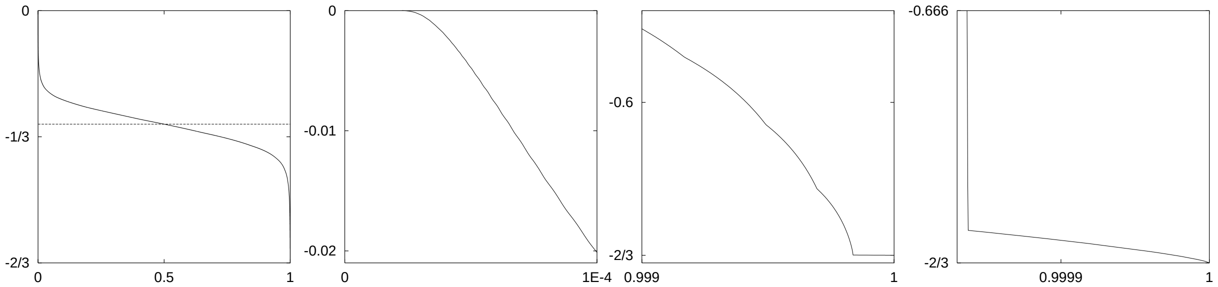

(a) (b) (c) (d)

Figure 7: The function $\Psi'(\Psi,\eta)$ for $\Psi = -0.3$ and $\varepsilon = 0.1$. (a): Plot in the full range $\eta \in [0,1]$; (b), (c) and (d) show different magnifications.

In figure 7 (c) and (d) a part of the numerically obtained plot $\Psi'(\Psi,\eta)$ is presented, $(1-\eta) \ll 1$. See figure 7 for the initial value of Ψ and the value of ε. The well seen break in the plot occurs at the critical value of η : $((1-\eta) = \varepsilon^3\Theta_0^{-1}(a/3)^4$. The small slope of the plot after the break is an artefact due to the choice of variables. In fact, the stretching in this region of η is very strong, as it can be seen from the following consideration.

At the point where the considered phase trajectory crosses the domain $\mathcal{D}_2$, one has $j = j_1$. One can see from (25) that j tends to 0^- as $(1-\eta) \to 0$ (corresponding to the surface of the sphere) and j tends to $-\infty$ as $(1-\eta) \to \varepsilon^3\Theta_0^{-1}(a/3)^4$ (corresponding to the centre of the sphere). Consider a segment PQ in $\mathcal{D}_1$ of a straight line $z = \text{const}$ (see figure 8). The point P lies on ON_1, and the point Q lies on OS_1. It follows from the above consideration that the part of the segment close to Q, corresponding to $\eta \in (1-\varepsilon^3\Theta_0^{-1}(a/3)^4, 1)$ is stretched in one iteration of the return map by a factor $\sim \varepsilon^{-4}$. The image of this part of the segment lies near the line ON_2 and its length is close to 1. The numerical illustration of this stretching is presented in subsection 6.1.2.

Dynamics in this case can be illustrated by figure 1 (b). Consider the point B inside of $\mathcal{D}_1$ close enough to OS_1. In the process of evolution it follows closely the stable manifold W_S^s and approaches the point S. Then it follows closely the one-dimensional unstable manifold $h_S^{u,2}$ (denoted in the figure as m_2), crosses the plane $z = 0$, and reaches the domain $\mathcal{D}_2$ at the point B′ situated very close to ON_2. The closer is B to the line OS_1, the closer is its image B′ to the point N_2.

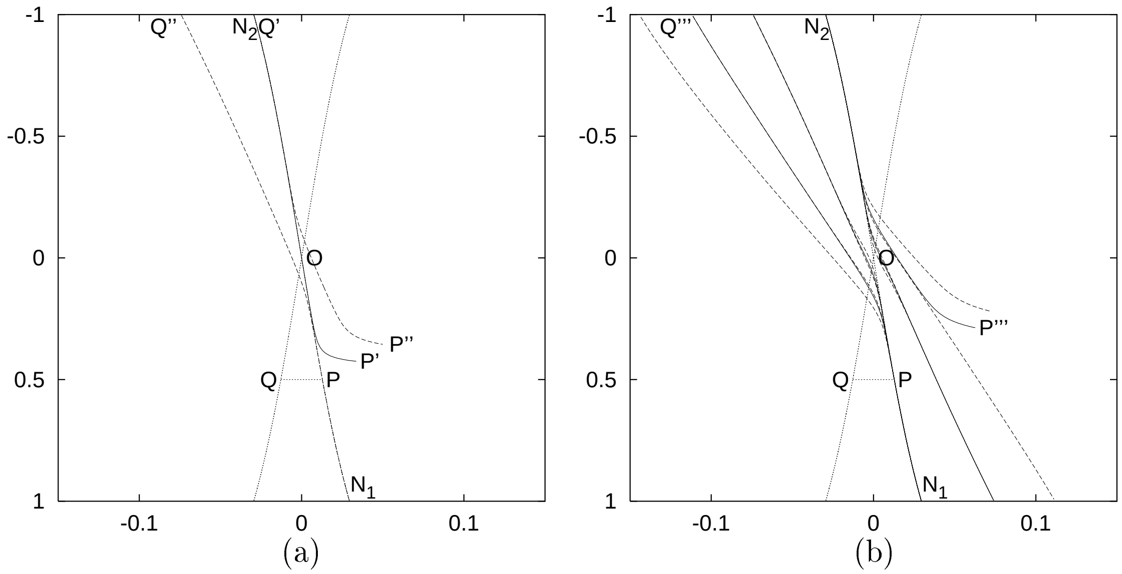

Figure 8: (a) A line, PQ, with $z = 0.5$ and the first two images, P'Q' and P"Q", under the Poincaré map. The image from P" to Q" consists of two pieces, one from P" to a point very close to N_2 and another from a point very close to N_1 to Q". (b) a similar plot for the third and fourth images of PQ. They consist, respectively, of 4 and 8 pieces.

5.2 Properties of the return map at $\eta \preceq \varepsilon^3$.

In this case the main change in the value of Φ occurs on the turn γ_0 of the phase trajectory. Consider a point A in the equatorial plane close to OS_1 outside of the domain $\mathcal{D}_1$ (see figure 1 (b)). At the point A we have: $I = i_A = -\varepsilon\Theta_A\bar{\eta} - \varepsilon\Theta_A/2$; $J = j_A$; $\bar{\eta} \preceq \varepsilon^3$; $\Theta_A = \Theta(j_A)$. Hence, at the point $\widetilde{\mathrm{M}}_0$ on this phase trajectory, we find $\tilde{i}_0 = -\varepsilon\Theta_A\bar{\eta}$; $\tilde{j}_0 = j_A$; $\tilde{l}_0 = -|\varepsilon\Theta_A\bar{\eta}|^{1/4}$; $\tilde{k}_0 = -|\varepsilon\Theta_A\bar{\eta}|^{3/4} j_A$. After the point $\widetilde{\mathrm{M}}_0$ the phase trajectory follows closely the unstable manifold $h_S^{u,1}$, denoted as m_1 in figure 1 (b). The change in the value of L on the segment $\widetilde{\mathrm{M}}_0\mathrm{M}_0$ is $\delta_1 l = \varepsilon a/3$ (see (16), (17)).

Therefore, we find at M_0:

$$\begin{aligned} l_0 &= -|\varepsilon\Theta_A\bar{\eta}|^{1/4} + \varepsilon a/3;\; k_0 = \tilde{k}_0, \\ i_0 &= -\left(|\varepsilon\Theta_A\bar{\eta}|^{1/4} - \varepsilon a/3\right)^4;\; j_0 = -k_0|l_0|^{-3} = |\varepsilon\Theta_A\bar{\eta}|^{3/4} j_A \left(|\varepsilon\Theta_A\bar{\eta}|^{1/4} - \varepsilon a/3\right)^3. \end{aligned} \tag{28}$$

The phase trajectory γ crosses the equatorial plane at the point A' belonging to $\mathcal{D}_1$. At this point we have:

$$\begin{aligned} j_{A'} &= j_0;\; i_{A'} = i_0 + \varepsilon\Theta_0/2;\; \Theta_0 = \Theta(j_0); \\ \eta &= (\varepsilon\Theta_0/2 - i_{A'})(\varepsilon\Theta_0)^{-1} = \left(|\varepsilon\Theta_A\bar{\eta}|^{1/4} - \varepsilon a/3\right)^4 (\varepsilon\Theta_0)^{-1}. \end{aligned} \tag{29}$$

Note, that the last expression implies that at arbitrarily small values of $\bar{\eta} > 0$, we have $\eta > \varepsilon^3\Theta_0^{-1}(a/3)^4$. The part of $\mathcal{D}_1$ where $\eta < \varepsilon^3\Theta_0^{-1}(a/3)^4$ is visited by phase trajectories that cross the separatrix right after crossing the plane $z = 0$ (i.e. those with $\widetilde{\mathrm{M}}_0$ at $z < 0$). This case is similar to the one considered in the previous subsection. The return map in this case will be considered below.

Using expansion (7) and (29), we find:

$$\Phi_{A'} = \Phi_0(j_0) - \frac{4}{3}a|j_A|2^{-3/4}\left[(\varepsilon\Theta_0)^{1/4} + \varepsilon\eta^{-1/4}a/3\right]^3. \tag{30}$$

From (28) and (29) it follows that if $\bar{\eta}$ is small enough and j_A is of order 1 or less, j_0 is close to zero. Expanding $\Phi_0(j_0)$ in (30) and using that $\Theta_0 \approx \Theta(0) = 3\pi/16$, we obtain in this case:

$$\Psi' = -\frac{3\pi}{16}|j_A(\Psi)|\left[1 - \varepsilon^{3/4}\eta^{-1/4}\frac{\pi^{1/4}}{4\cdot 3^{1/4}}\frac{\Gamma(5/8)}{\Gamma(9/8)}\right]^3, \quad \eta > \frac{16\varepsilon^3}{3\pi}\left[-\frac{a}{3}\right]^4. \tag{31}$$

This is the first equation of the return map. The second equation in this case is the same as in (18), because it generally takes $\sim 1/\varepsilon$ iterations of the Poincaré map for the point A$'$ to reach the domain $\mathcal{D}_2$.

If $\eta < \varepsilon^3\Theta_0^{-1}(a/3)^4$, the turn γ_0 of the phase trajectory crosses the plane $z = 0$ at a point where $\Psi = -2/3 + \mathrm{O}(\varepsilon^{3/4})$. The value of K at this point is, as it follows from (22), $k = 3(\Psi + 2/3)/(4a)$. As K is well-preserved on the segment of the trajectory between the plane $z = 0$ and M_0, we have $k_0 = k = -|i_0|^{3/4}j_0$. On the other hand, $i_0 = -\varepsilon\Theta_0\eta$. Therefore, one obtains

$$j_0 = -3(\Psi + 2/3)a^{-1}|\varepsilon\Theta_0\eta|^{-3/4} \tag{32}$$

Using expansion (7), we find in the main approximation

$$\Psi' = \Phi_0(j_0) + \Psi + 2/3 = -2/3 + 2Z^2\int_0^1 v\sqrt{(1-v)(1+v+v^2-Z^2v^2)}dv, \tag{33}$$

where $0 < Z < 1$ is a root of the equation $j_0z^3 - z^2 + 1 = 0$, and $j_0(\Psi)$ is implicitly given by (32). The second equation of the return map in this case is the same as in (18).

In figure 7 (b) a part of the numerically obtained plot $\Psi'(\Psi, \eta)$ is presented, $\eta \ll 1$. The initial value $\Psi = -0.3$ is not close enough to $-2/3$. Therefore the plot does not have points at values of η less than the critical value of $\eta = \varepsilon^3\Theta_0^{-1}(a/3)^4$. One can see both from the figure and from expression (31) that the slope of the plot tends to zero as η tends to this critical value from the right. This implies that the stretching properties of the return map decrease in this region.

6 The properties of the return map obtained numerically, and comparison with theoretical predictions

It was shown in Section 4 that in the part of the fundamental domain not too close to its boundary the return map has strong stretching properties. As it was shown in Section 5, the stretching property weakens near the part of the boundary where η is close to 0, i.e. near the line ON_1 and near the line $\mathrm{S}_1\mathrm{N}_1$ where Ψ is exponentially small. However, as it happens only on a small region of measure $\mathrm{O}(\varepsilon^3)$, a typical trajectory does not visit this region for a long time ($\sim \varepsilon^{-3}$ iterations of the return map or $\sim \varepsilon^{-4}$ units of time). Hence, for this time interval the motion is similar to that in a hyperbolic system. The standing question is if visits to this small neighbourhood of the boundary can spoil the hyperbolic behaviour. Therefore, the search for possibly existing islands of stability is necessary. In this section, we check numerically hyperbolic properties and ergodic behaviour of the system and compare results with theoretical predictions. Only a small sample of the tests done is presented here. Finally we discuss a simple approach to find islands and we show some extremely small examples. We comment on the difficulties to find these islands for small values of ε and on the relevance they have.

Any point in $\mathcal{D}_1$ being on W^s_S will end on S under forward flow. As a first question we find the points in $\mathcal{D}_1$ such that they enter S before reaching $\mathcal{D}_2$. On these points the return map $\nu\mu$ is not defined. They can be obtained as preimages, in $\mathcal{D}_1$, of the line OS_2. Figure 9 (a) shows these preimages, a countable set of lines going from the ON_1 line to the intersection of m_4 with the equator, very close to S_1 (see figure 1 (b)). These are the discontinuity lines for $\nu\mu$. Note that in this figure, and most figures in this section, the positive z axis points downwards. Close to the circle boundary some of these lines are shown in figure 9 (b), using (η, ρ) variables, where $\rho = (x^2 + z^2)^{1/2}$. See the beginning of section 6.1 for the meaning of the black zones in this plot.

We can consider $\mathcal{D}_1$ split by these lines in different regions, to be denoted as $\mathrm{Q}_1,\mathrm{Q}_2,\ldots,\mathrm{Q}_j,\ldots$ from top to bottom in the figure, that is, Q_1 is the region closer to (0,0). Note that the points in Q_j arrive to $\mathcal{D}_2$ by μ in j iterates of the Poincaré map with respect to the equatorial plane. The image of Q_j under $\nu\mu$ is the set, $S_z(\mathrm{Q}_j)$ obtained by symmetry with respect to the z axis.

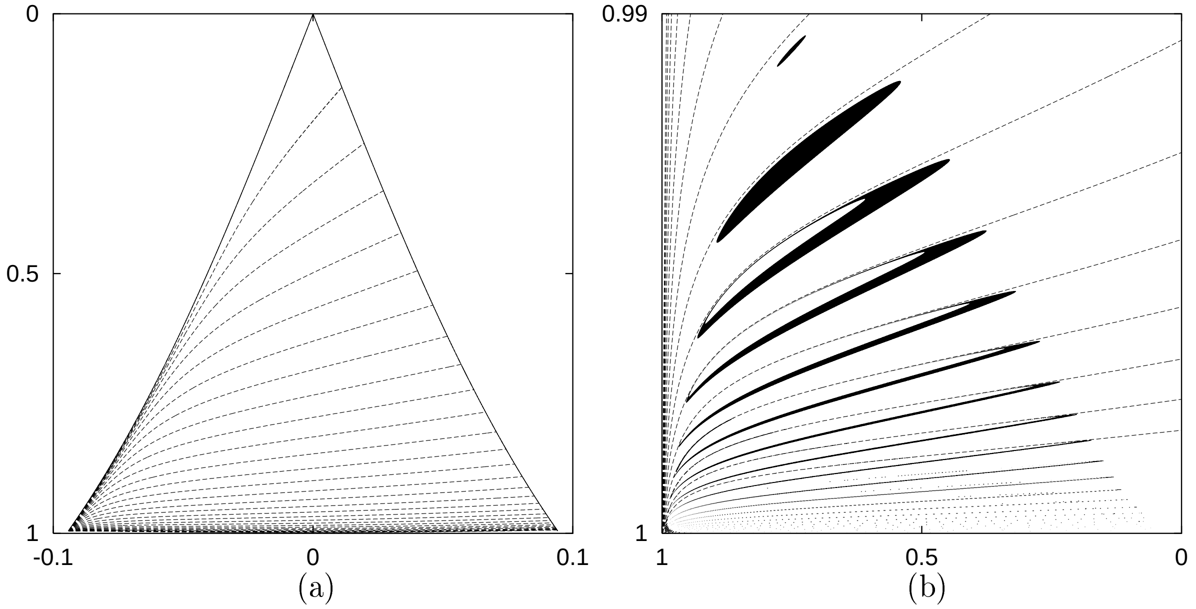

Figure 9: (a) Lines where $\nu\mu$ is discontinuous in $\mathcal{D}_1$ shown in (x, z) variables, computed for $\varepsilon = 10^{-1/2}$. (b) A magnification near the boundary, showing some lines in (η, ρ) variables. See the text.

6.1 Hyperbolic properties

Here we present illustrations of the stretching and compressing properties of the return map. To this end the differential of $\nu\mu$, $D(\nu\mu)$, is computed. In most of $\mathcal{D}_1$, $D(\nu\mu)$ is an hyperbolic matrix, but not everywhere. In 6.1.1 we show the field of unstable and stable directions of $D(\nu\mu)$ and the integral lines of this field. In 6.1.2 the images of lines $z =$ const are shown, and the stretching properties are discussed.

The computation of $D(\nu\mu)$ involves an important detail. The return map has an invariant measure, but this is a smooth deformation of the Lebesgue measure, μ_L, on the wedge. It is convenient, to be able to talk about "elliptic zones", to modify the map so that it preserves μ_L. This is easily done by changing the variables as follows. Instead of (x, z) we shall use new variables $(\hat{x}, \hat{z}) = G(x, z)$ defined as $\hat{x} = 3x - 11x^3/3 - xz^2$, $\hat{z} = z$. Let $(x^*, z^*) = \nu\mu(x, z)$. Then it is immediate to check that the map $\mathcal{A} = G\nu\mu G^{-1}$ preserves

μ_L. The purpose of G is just to cancel the effect of the y component of the vector field. However, all the examples will be presented in the (x, z) or some related variables, as η or ρ. In particular, if $\mathcal{A}$ is hyperbolic at some points, the eigenvectors are computed in $(\hat{x}, \hat{z})$ and then sent to the (x, z) variables by DG^{-1}.

As first example we comment on the black zones of figure 9 (b). The map $D\mathcal{A}$ is hyperbolic everywhere in $\mathcal{D}_1$ except in these black zones. Even taking a big value of ε as $10^{-1/2}$, the first black zone appears in Q_{23}. Let us denote as B_j the black zone in Q_j. The image of B_j is $S_z(\mathrm{B}_j)$. Note that, except the first two black zones, Q_{23} and Q_{24} in figure 9 (b), the remaining ones have a white zone inside. On them $D\mathcal{A}$ is hyperbolic with reflection.

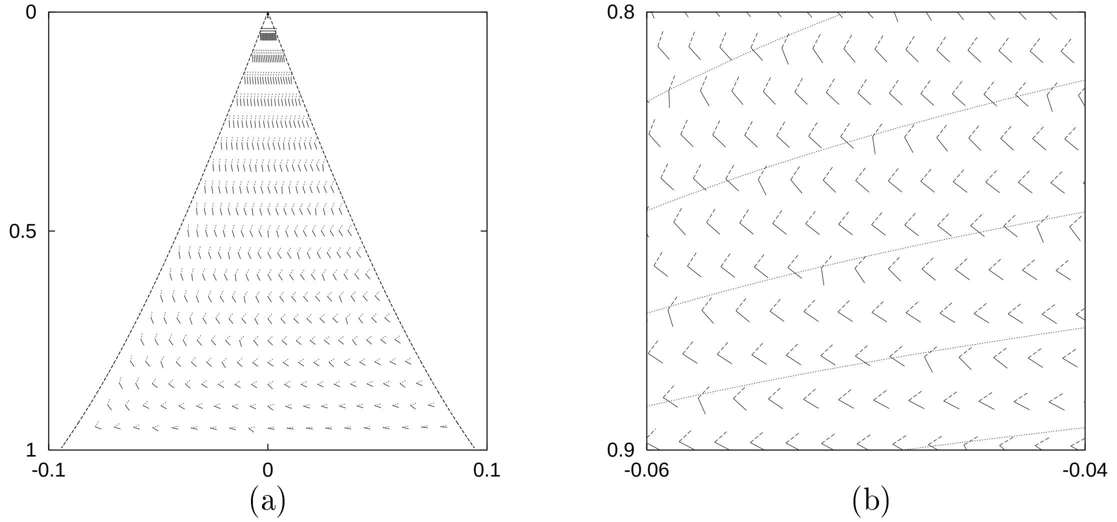

Figure 10: (a) Directions of the unstable (continuous line) and stable (broken line) eigenvectors for $\varepsilon = 10^{-1/2}$. (b) A magnification of (a) showing also the discontinuity lines of the return map. The (x, z) coordinates have been used.

6.1.1 Eigen directions and eigenvalues of the return map

Figure 10 shows the eigen directions (unstable and stable) of the return map, computed as described above. Note that the angle between them decreases, in most of the points, when z increases. Both eigenvalues and eigen directions become discontinuous at the discontinuity lines. The changes in the eigen directions can be seen in the (b) part of the figure. The slope of the unstable directions becomes very big when a discontinuity line is approached from below (that is, from larger z to smaller z).

A better visualization of this behaviour is shown in figure 11, drawn for the same value of ε by using $z = 0.994$. Check figure 9 to see that, for this z there are intersections with B_{24} and B_{25}. Let λ be the dominant eigenvalue of $D\mathcal{A}$. The continuous line gives the $\log(\lambda)$ if $|\lambda| > 1$. Otherwise it gives $\log(|\mathrm{Re}\,\lambda\,|)$. Variable ξ has been used in the horizontal axis. The spikes in $\log(\lambda)$ appear at the discontinuity lines. Check that going from $\xi = 0.5$ to $\xi = 1$ and just before the first spike in this range (going from right to left), one encounters a passage through an elliptic zone, followed by a passage through a hyperbolic with reflection zone and a short passage again through an elliptic zone. This corresponds to crossing B_{25}. Later on we find the crossing of B_{24}, this time without hyperbolic with reflection zone.

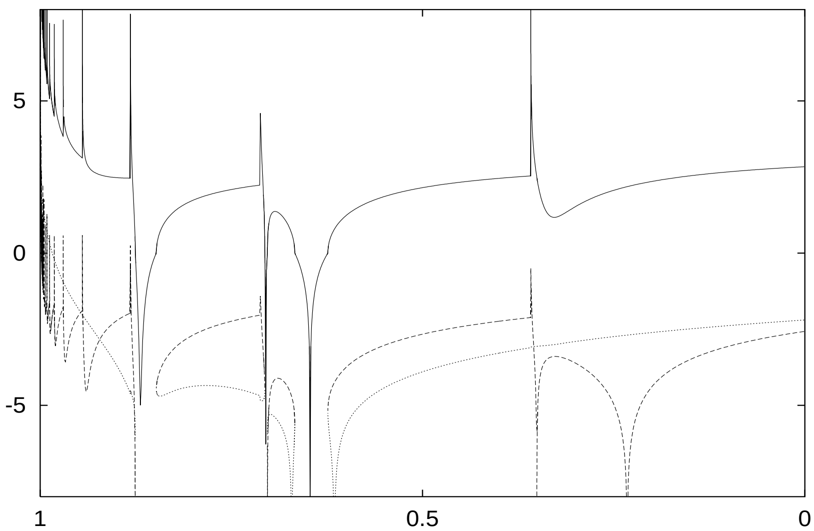

Figure 11: Dominant eigenvalue and slopes of the eigen directions, all of them in logarithmic scale, for $\varepsilon = 10^{-1/2}$ and $z = 0.994$. The horizontal variable is ξ. See the text for additional information.

The slopes of the unstable (resp. stable) directions are shown (also in log scale) as broken lines (resp. dotted lines). They are absent in the elliptic zones. Despite the eigenvalue goes to infinity at one side of the discontinuity lines (remaining finite at the other side), the slopes tend to finite values at the both sides. In fact the jumps of the stable directions are hard to detect in the plot.

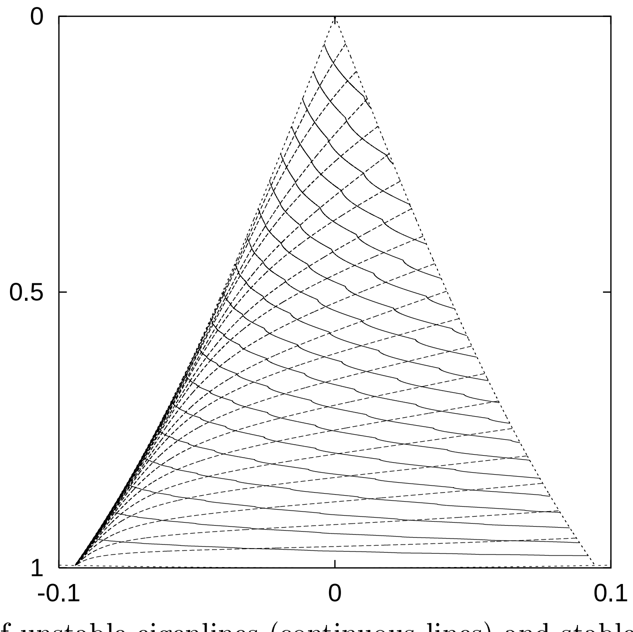

Figure 12: A sample of unstable eigenlines (continuous lines) and stable eigenlines (discontinuous lines) on a fundamental domain.

Finally, figure 12 shows integral curves of the fields of unstable and stable directions. The stable lines look very similar to the discontinuity lines. In fact the stable lines never cross a discontinuity line, they remain on a fixed Q_j domain. On the other side, each unstable line crosses a finite number of Q_j domains. Note that the image of a stable line in Q_j under the return map is the symmetric under S_z of the part of an unstable line inside Q_j. Vice versa: the image of the part of an unstable line in Q_j is the symmetric under S_z of a stable line in Q_j. Except for the presence of the elliptic zones, this would be an ideal situation to show the global hyperbolicity of the map $\mathcal{A}$.

6.1.2 Images of lines in the fundamental domain

Consider in the fundamental domain $\mathcal{D}_1$ a segment PQ of a straight line $z = \text{const}$ (see figure 8 (a), $z = 0.5$). The point P lies on ON_1, and the point Q lies on OS_1. Consider also a point R on PQ close to Q but still at a distance of order ε from Q. The variation of the function Φ along PQ is a value of order $\varepsilon^{3/4}$.

For the points on PR the change in Φ in the process of receding from the separatrix during the motion in system (1) is a value of order $\varepsilon^{3/4}$. Before arrival to the domain $\mathcal{D}_2$ these points move during a time $\sim 1/\varepsilon$. As a result of this motion the image of PR under the return map is expanded by $\sim \varepsilon^{-1/4}$ times with respect to PQ and consists of $\sim \varepsilon^{-1/4}$ pieces (see figure 13 (a)). For every such piece, the endpoint on OS_1 has a value of z-coordinate $\mathrm{O}(\varepsilon^{3/4})$-close to the initial one. The endpoint on ON_1 has a value of the z-coordinate close to 1 (as it has $\bar{\eta} = 0$ at the Poincaré iterate preceding its arrival to $\mathcal{D}_2$, and the correspondent value of $j = 0$ (see (28), (29)), which corresponds to the surface of the sphere.

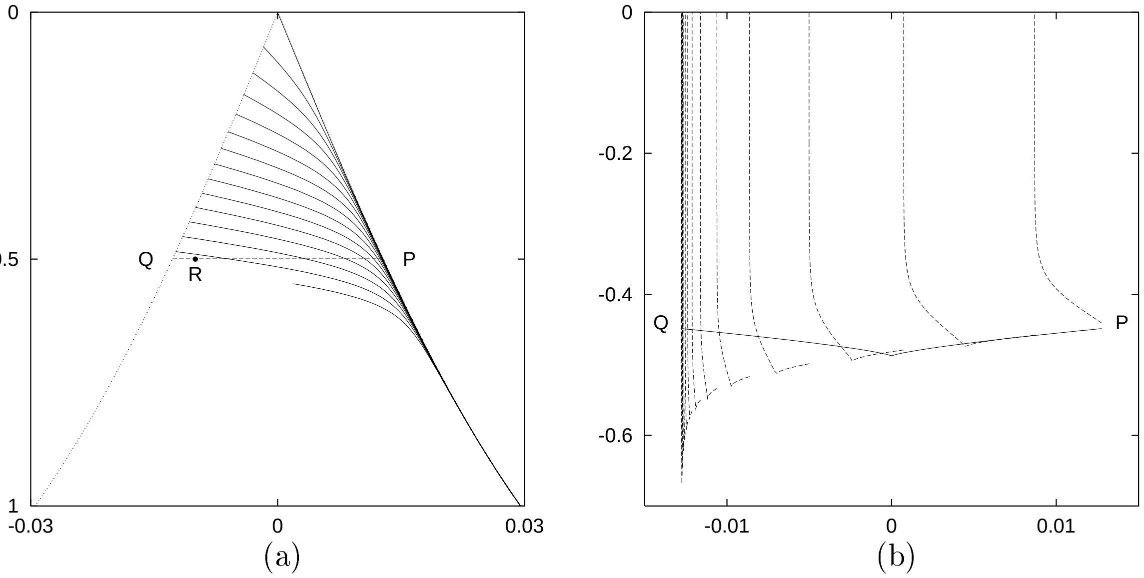

Figure 13: (a) Image of the line $z = 0.5$ in $\mathcal{D}_1$ under the return map for $\varepsilon = 10^{-1}$, in the (x, z) coordinates. (b) Same image with the final value of Φ as a function of the initial value of x.

For points of RQ that are $\mathrm{O}(\varepsilon^4)$ close to Q, the change in Φ in the process of receding from the separatrix is a value of order 1 (as the trajectory passing through Q tends to the south pole of the unit sphere, and the corresponding value of Φ tends to 0. Therefore, the image of RQ under the return map is expanded $\sim 1/\varepsilon$ times with respect to PQ and consists of $\sim 1/\varepsilon$ pieces.

The stretching properties of the return map are also illustrated by figure 13 (b). In the figure, one can see the initial segment PQ drawn in coordinates x, Φ (the continuous line). The dotted line shows the value of Φ in the image of the segment over initial x-coordinate on PQ. Each component of the dotted line corresponds to a component of the image of the segment PQ. One can see that the regions of very strong stretching are separated by those where the stretching is weaker.

6.2 Ergodic properties

6.2.1 Number of visits to the fundamental domain

It looks reasonable to suppose that due to (partly) hyperbolic properties of the return map the motion inside the sphere is ergodic, at least up to small measure. A long trajectory spends in any measurable set a time proportional to the volume of this set. Consider the Poincaré map with respect to the equatorial plane. This map should also be close to ergodic: for any measurable set in the equatorial plane the number of arrivals to this set should be approximately proportional to the measure of this set, i.e., to the phase flux of the vector field (1) through this set.

Consider as a test set the union of the fundamental domains $\mathcal{D}_1 \cup \mathcal{D}_2$. The phase flux through them is, in the leading approximation,

$$\mathrm{Fl}_1 = \int_{D_1 \cup D_2} \mathrm{d}i\mathrm{d}j = 2\int_{D_1} \mathrm{d}i\mathrm{d}j = 2\varepsilon \int_0^\infty \Theta(j)\mathrm{d}j = 2\varepsilon\left(\Phi_0(\infty) - \Phi(0)\right) = \frac{4}{3}\varepsilon.$$

The flux through the equatorial plane in the "upwards" direction is equal to the flux through the intersection of the interior of the unit circle and interior of the ellipse $\mathcal{E}$. Integrating the function $(11x^2 + z^2 - 3)$ over this area, one obtains for this flux:

$$\mathrm{Fl}_2 = 2 + \frac{9}{\sqrt{11}} \arctan\frac{2}{\sqrt{11}} \approx 3.473\,.$$

Therefore, in a long sequence of the Poincaré map iterations the ratio of arrivals to $\mathcal{D}_1 \cup \mathcal{D}_2$ to the number of iterations should be approximately equal to $\mathrm{Fl}_1/\mathrm{Fl}_2 \approx 0.384\varepsilon$. This agrees with results of numerical simulations, provided the sequence of iterates is long enough.

In figure 14 the plots show the number of visits to $\mathcal{D}_1 \cup \mathcal{D}_2$ as a function of the number of visits to the intersection of the interior of the unit circle and the interior of the ellipse $\mathcal{E}$. Let N_P be the final number of Poincaré iterates in a run and n_W the number of passages through the wedges up to the Poincaré iterate number n_P. The horizontal axis displays $\mathrm{n}_P/\mathrm{N}_P$ and the vertical one shows $\mathrm{n}_W/(\varepsilon\mathrm{N}_P)$. The different lines correspond to values of N_P equal to 10^k for $k = 5, 6, 7, 8$, shown as a dotted line, a broken line with short segments, a broken line with long segments and a continuous line, respectively. The part (a) has been produced for $\varepsilon = 0.1$, while (b) uses $\varepsilon = 0.01$. The initial values are irrelevant. They have been taken as $x = 0.05$, $z = 0.5$. Note that in (a) the cases $\mathrm{N}_P = 10^7$ and $\mathrm{N}_P = 10^8$ are almost equal. On the other hand, case (b) shows big variations, depending on N_P. The final number of visits is N_W =3,829,162 in case (a), giving a frequency 0.03829 quite close to the limit one, while in case (b) we have N_W =368,708, i.e., a frequency 0.003687 with a 4% relative error. This is coherent with the requirement that the number of iterates must be a (large) multiple of ε^{-4} to have good statistics. This effect is more dramatic if ε is decreased. This will be illustrated by figure 17, where $\varepsilon = 10^{-3}$ has been used.

6.2.2 Distribution of points inside the fundamental domain

The return map has an invariant measure $\mathrm{d}m$ which can be approximated by $(3-z^2)\mathrm{d}x\,\mathrm{d}z$ for small ε, and the width of the wedge in x is essentially proportional to z (see sections

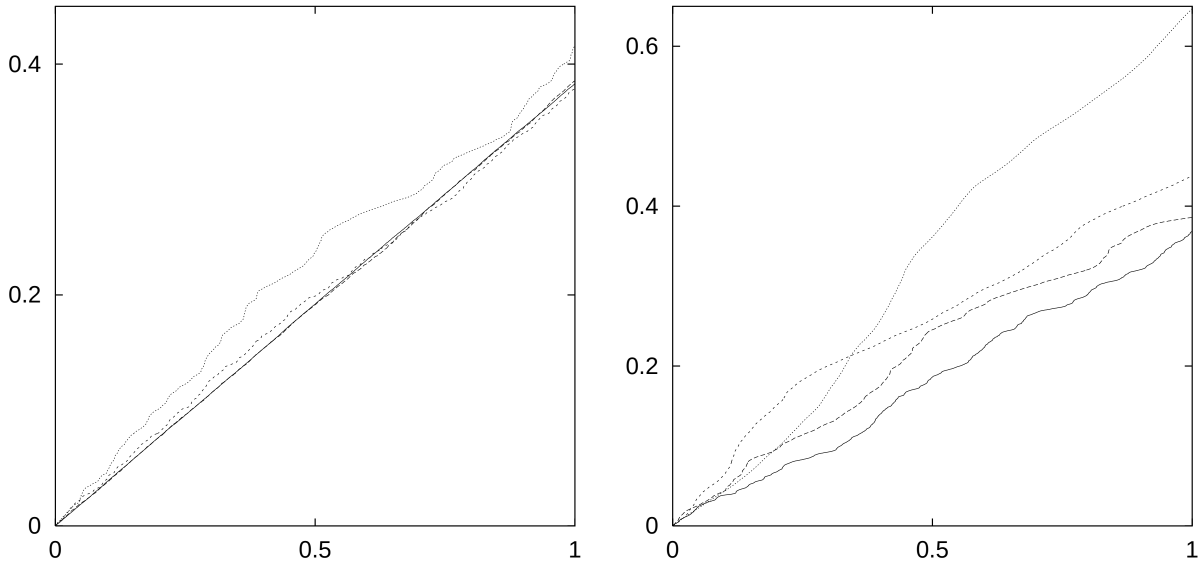

Figure 14: Number of passages through the wedges versus number of Poincaré iterates. Both numbers have been normalised (see text). (a) corresponds to $\varepsilon = 0.1$ and (b) to $\varepsilon = 0.01$. The different lines are the results for a final number of Poincaré iterates equal to 10^k, $k = 5, 6, 7, 8$.

3 and 4). It follows that the normalised density of points on the wedge, if we disregard minor effects of x and look only at the value of z, is $\frac{4}{5}z(3 - z^2)$.

To test this theoretical distribution several runs have been made. The values used for ε are $10^{-k/2}$ with $k = 1, 2, 3, 4, 5$. For each value 10 initial conditions of the form $z = 0.1$, $x = m \times 0.05$, $m = 1, \ldots, 10$ have been taken. For each one of these conditions the vector field has been integrated until a number of 10^6 passages through the wedge has been reached. For relatively large ε there are no significant differences between the 10 runs. Figure 15 shows the cumulative results, taking the 10 runs together. In (a) we present the experimental density, as a function of z for $\varepsilon = 10^{-k/2}$, $k = 1, 2, 3$ using continuous line for $k = 1$, broken line for $k = 2$ and dotted line for $k = 3$. In (b) these lines are used for $k = 4$, $k = 5$ and the theoretical value, respectively. Even averaging over the 10 runs, we see that the distribution, especially for $k = 4$, $k = 5$ is still far from the theoretical one, while in (a) the agreement is good, mainly for $k = 0$, $k = 1$. As one can expect, the largest deviations are produced near $z = 1$.

6.3 Distribution of jumps in the adiabatic invariant

The numerically found distribution function of $\Delta\Phi$ in a long sequence of separatrix crossings is shown in figure 16. Under the hypothesis of ergodicity of the return map one can obtain approximate formula for this distribution using the formula (10) for $\Delta\Phi$.

Introduce

$$D = -\Gamma(1/4)a^{-1}\varepsilon^{-3/4}\Delta\Phi = \Theta^{3/4} j f(\xi), \tag{34}$$

where for brevity we used the notations $\Theta = |\Theta_*|, j = |j_*|$ and all the other components in the leading term of (10) are denoted by $f(\xi)$. According to Section 4, the density of the invariant measure of the return map in the wedge $\mathcal{D}_1$ is proportional to the density of the phase flux of the vector field (1) through $\mathcal{D}_1$. One can use as coordinates in $\mathcal{D}_1$ the values $\xi, \Phi_0(j), \xi \in (0, 1), \Phi_0(j) \in (-2/3, 0)$. In the main approximation the density of invariant

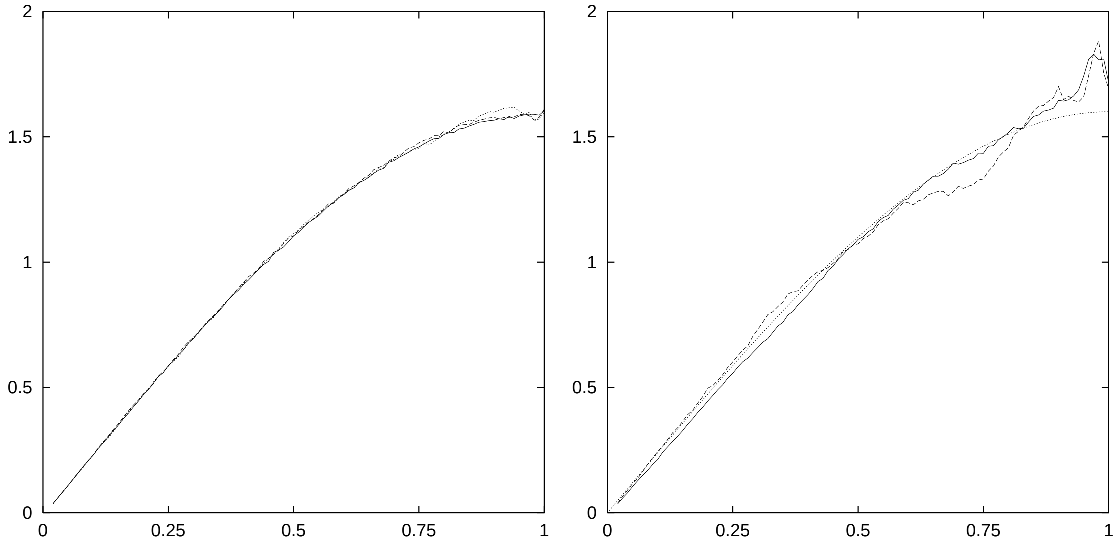

Figure 15: Experimental density of the distribution of the values of z on the wedge. (a) The values for $\varepsilon = 10^{-1/2}$, 10^{-1} and $10^{-3/2}$. (b) The values for $\varepsilon = 10^{-2}$, $10^{-5/2}$ and the theoretical density.

measure in these variables is constant (3/2). In probabilistic terms this means that the values ξ and $\Phi_0(j)$ are independent, and they have uniform distributions. Therefore, the density of conditional distribution of value D (34) at fixed j is $(\Theta^{3/4} j f'(\xi))^{-1}$, where $f' = \mathrm{d}f/\mathrm{d}\xi$. Integrating this density over $\kappa = 3\Phi_0(j)/2$ from -1 to 0, changing the integration variable from κ to j and recalling that $\mathrm{d}\Phi_0/\mathrm{d}j = \Theta(j)$, we find the probability density for D:

$$p(D) = -\frac{3}{2}\int_{-\infty}^{0} \frac{\Theta^{1/4}\,\mathrm{d}j}{j f'\left(f^{-1}\left(\frac{D}{j\Theta^{3/4}}\right)\right)}, \tag{35}$$

where f^{-1} is the function inverse to f. Changing the variable of integration from j to z we obtain:

$$p(D) = -\frac{3}{2}\int_{0}^{1} \frac{\Theta^{1/4}(z)}{f'\left(f^{-1}\left(\frac{D}{j(z)\Theta^{3/4}(z)}\right)\right)} \cdot \frac{3-z^2}{z(1-z^2)}\,\mathrm{d}z, \tag{36}$$

where $\Theta(z)$ is defined in (9), and $j(z) = (z^2-1)/z^3$. Under the hypothesis of ergodicity, the distribution of the value $(-\Gamma(1/4)a^{-1}\varepsilon^{-3/4}\Delta\Phi)$ in a long sequence of separatrix crossings should tend to $p(D)$ as the length of the sequence tends to ∞.

Function $p(D)$ (36) has a singularity at $D = 0$. This singularity comes from the singularity of the integrand at $z = 1$. It is straightforward to obtain the main term in $p(D)$ at small D:

$$p_0(D) = \frac{3}{2}\Theta^{1/4}(1)\frac{\ln|D|}{f'(1/2)} = -\frac{3}{2}(-1+2^{5/4})(3\pi)^{1/4}\Gamma\left(\frac{5}{4}\right)\zeta\left(\frac{5}{4}\right)\ln|D| \approx -15.086\ln|D|, \tag{37}$$

where $\zeta(\cdot)$ is the Riemann zeta function.

To check the predicted behaviour we have used the same samples already used in figure 14. The figure 16 shows the results. Even for $\varepsilon = 0.01$ there is a very good agreement with the theoretical distribution after 10^8 Poincaré iterates. On the other side it is clear that 10^6 iterates are not enough to approach the limit density if $\varepsilon = 0.01$, while they produce already nice results for $\varepsilon = 0.1$.

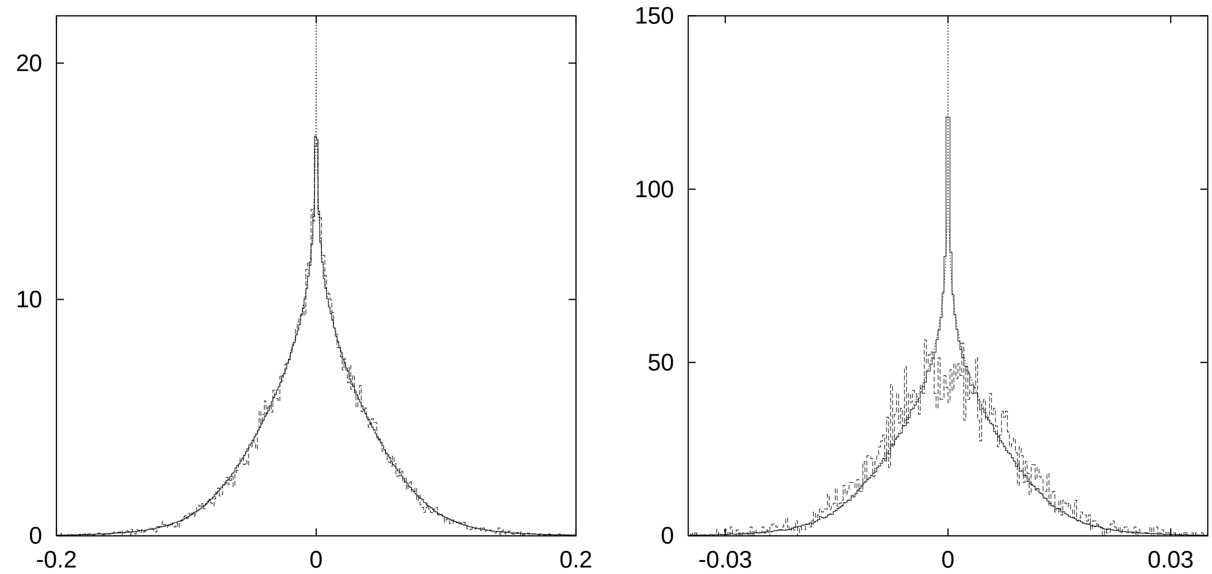

(a) (b)

Figure 16: Distribution of jumps of the adiabatic invariant. (a) Computations for $\varepsilon = 0.1$. (b) Computations for $\varepsilon = 0.01$. The dotted lines represent the theoretical distribution given by (36). The continuous lines correspond to the values after 10^8 Poincaré iterates, while the broken lines give the experimental distribution after 10^6 Poincaré iterates.

To see the effect of using small values of ε on the statistical properties figure 17 displays some results for $\varepsilon = 10^{-3}$. The starting point is, as before, $x = 0.05$, $z = 0.5$. The dotted line in (a) shows the distribution of visits for the first 10^6 Poincaré iterates. The jumps are very small and it looks as a line with constant slope. This is essentially true for every block of 10^6 consecutive iterates along the run with very few exceptions. The short broken line, going up to 10^7 iterates has a large increase. This corresponds to a large period close to $\Phi = -2/3$ (compare with (c), where the values of Φ are plotted as a function of the number of the iterate). The curve shown as solid line goes up to 10^9 iterates and gives a final number of visits to the wedge equal to 410,631. The average frequency still has a relative error near 7% after this large number of iterates. A few regions of relatively large increase of the number of visits are easily identified in (c) as large periods near $\Phi = -2/3$.

Note that no passages sufficiently close to $\Phi = 0$ have been found. This explains why the experimental density of jumps fails to give an approximation of the singularity at $D = 0$. In fact, for 10^7 and 10^8 iterates (last one plotted in (b) using broken lines) the distribution is closer to a normal one, with standard deviation near $\sigma = 0.00163$ than to the distribution with density (36). For 10^9 the pattern approaches the theoretical one and is definitely different from a normal one. Using 10^6 gives a too wild density distribution.

In figure 17 (c) one could use, instead of the current value of Φ, the value of $|z|$ or simply the number of Poincaré iterates between two successive passages through $\mathcal{D}_1 \cup \mathcal{D}_2$. All these plots are quite similar.

6.4 Correlation function of the jumps in the adiabatic invariant

To test the assumption about the independence of successive jumps, it is suitable to compute the autocorrelation function of the jumps in Φ. That is, the correlation $\rho(s)$ of

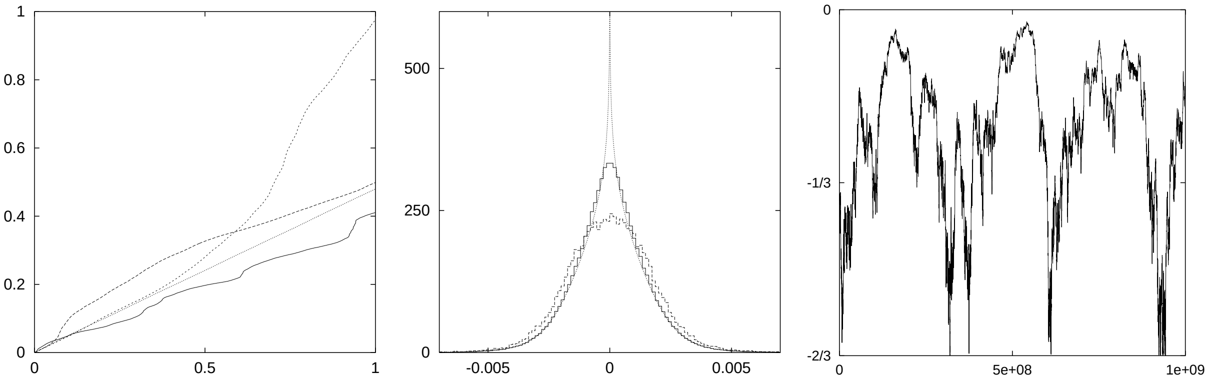

(a) (b) (c)

Figure 17: An illustration of the bad statistical properties for $\varepsilon = 10^{-3}$ after 10^9 Poincaré iterates. (a) The scaled number of visits to the wedge after 10^k iterates, $k = 6, 7, 8, 9$. (b) The distribution of the jumps of the adiabatic invariant Φ. The theoretical density is compared to the experimental values after 10^8 and 10^9 iterates. (c) The current value of Φ as a function of the number of the iterate. See the text for comments.

the variables $X(n) = \Phi(n)$ and $Y(n) = \Phi(n+s)$, where n denotes the successive passages through $\mathcal{D}_1 \cup \mathcal{D}_2$ and s is some fixed shift taking as values natural numbers. Of course, $s = 0$ gives $\rho(0) = 1$, and the assumption implies that $\rho(s) \to 0$ when the size of the sample N_W tends to ∞, for any fixed value of $s > 0$.

We show in figure 18 some results for the same samples used in figure 14. In part (b), for $\varepsilon = 0.01$ it is clearly seen the tendency towards $\rho(s) = 0$ when $\mathrm{N}_W \to \infty$. Despite for $\mathrm{N}_W = 10^6$ the values of $\rho(s)$ are still large (of the order of 0.05 at most), for $\mathrm{N}_W = 10^8$ they decrease below 0.005. In part (a), however, these values decrease to 0.015 and 0.0015, respectively, for values of s greater than 200. But for small positive values of s the limit seems to be small but definitely different from $\rho(s) = 0$. Based on a moderate amount of experiments, it seems that $\rho(1)$ tends to some value, depending on ε and going quickly to 0 with ε. This behaviour is similar for small values of s, but the limit is going faster to zero when s increases.

This can be interpreted as follows. For ε large enough the jumps in Φ can be quite large. After a big positive jump the probability for the next jump is biased towards negative jumps and vice versa. This will lead to $\rho(s) < 0$ for small positive s.

6.5 Closed trajectories of the perturbed system

Some very simple closed orbits of (1) can be obtained by looking for initial conditions on $x = 0$. If a point of the form $(0, z^*) \in \mathcal{D}_1$ reaches $\mathcal{D}_2$ at $(0, -z^*)$ then the orbit is periodic. If the number of required Poincaré iterates is odd then the orbit passes through a point of the form $(\bar{x}, 0)$ outside the ellipse $\mathcal{E}$. If it is even it passes through a similar point inside $\mathcal{E}$. Hence, it is enough to compute the orbit from $(0, 0, z^*)$ till the plane $z = 0$ is reached, looking for points such that the y value in this intersection is 0. Furthermore, it is possible to obtain the full monodromy matrix computing just this part of the orbit, by using the symmetries.

The location of successive values of z^* that correspond to periodic orbits is shown in figure 19 for three different values of ε. The successive numbers of Poincaré iterates are $n_P = 1, 2, \dots$. We have plotted the first 550, 170 and 55 solutions found for $\varepsilon =$

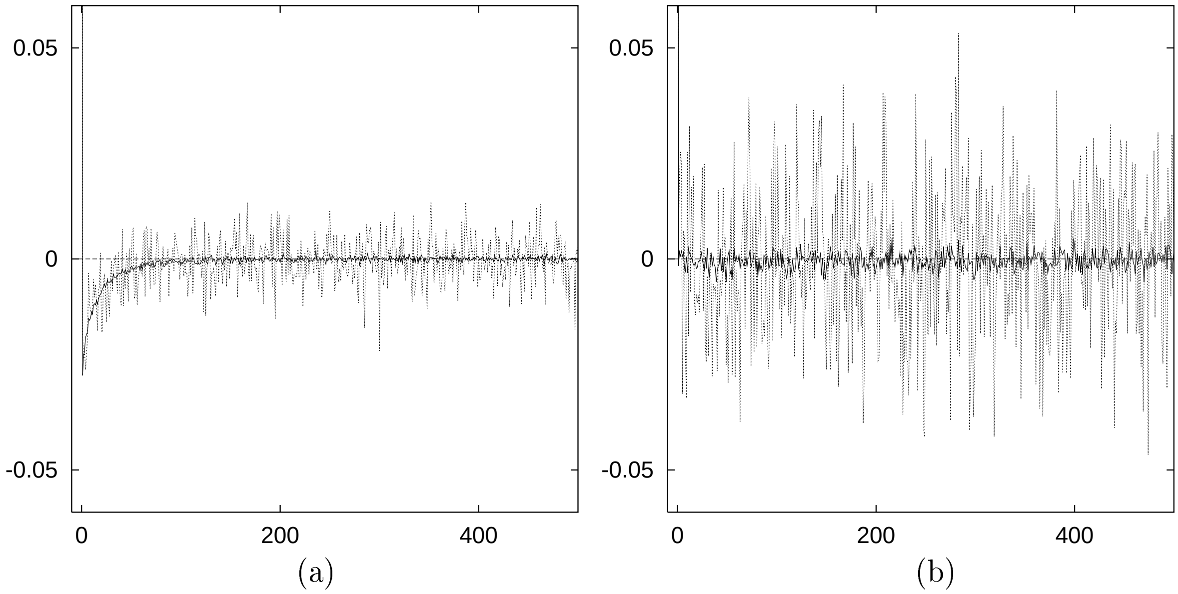

Figure 18: Autocorrelation function of the jumps in Φ. (a) displays results for $\varepsilon = 0.1$. (b) for $\varepsilon = 0.01$. The solid line is obtained using a total number of Poincaré iterates equal to 10^8. The broken lines use 10^6.

$10^{-1/2}$, 10^{-1} and $10^{-3/2}$, respectively. The last orbits displayed have values of z^* close to 0.999998 . The values of z^* tend to 1 in a geometric way with respect to n_P. The periods, in all cases, are roughly proportional to n_P, even independent of ε, except for small values of z^*.

These results are in agreement with estimates that one can obtain using the map (18). Indeed, for a stationary point number n_P with $\eta = \eta' = 1/2$ one finds from (18) in the main approximation: $\Omega(\Psi_{n_P}) = n_P\varepsilon$ with Ω defined in (19). At n_P sufficiently large the value Ψ_{n_P} is close to zero, and the corresponding phase trajectory on its way from $\mathcal{D}_1$ to $\mathcal{D}_2$ passes close to the saddle-foci of the system. Let Ψ_{n_P} be not exponentially close to 0. Then, one can estimate $\tau_*(\Psi_{n_P})$ in (19) as $\tau_*(\Psi_{n_P}) \sim -\ln|\Psi_{n_P}|$. Hence, $\Omega(\Psi_{n_P}) \sim -\ln|\Psi_{n_P}|$, and $|\Psi_{n_P}| \sim \exp(-n_P\varepsilon)$, giving the position of the stationary point. Note also that $t_* = \varepsilon^{-1}\tau_* \sim n_P$.

Any of these periodic orbits is a fixed point under $\mathcal{A}$ (see Section 6.1). A remarkable fact is that the traces of the differential of this map seem to behave in a quite regular way (see figure 19). These traces seem to tend to some finite value when $z^* \to 1$. As we shall see in the next subsection this is not the case, and there are stable periodic solutions at z^* exponentially close to 1.

These traces can also be easily estimated with the use of (18). For the trace of the differential of the map $\mathcal{P}\mu$ at one of the stationary points under consideration one finds in the main approximation

$$\mathrm{Tr} \sim \frac{1}{\varepsilon^{1/4}} \frac{\mathrm{d}\Omega}{\mathrm{d}\Psi} \frac{\partial h}{\partial \eta},$$

where the partial derivatives are calculated at $\Psi = \Psi_{n_P}$, $\eta = 1/2$. The value $\partial h/\partial \eta$ is proportional to $|j_*|$ (see (10)). At n_P sufficiently large, we have $j_*(\Psi_{n_P}) \approx \Psi_{n_P}/\Theta(0)$, $\Omega(\Psi_{n_P}) \sim -\ln|\Psi_{n_P}|$ (again, here we assume that Ψ_{n_P} is not exponentially close to 0). Therefore, $\mathrm{Tr} \sim \varepsilon^{-1/4}$ and does not depend in the main approximation on n_P. For the

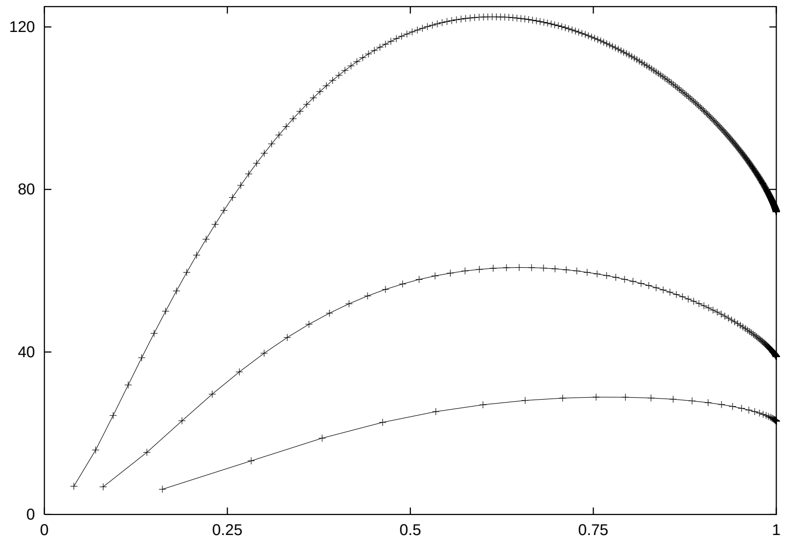

Figure 19: Hyperbolic periodic orbits on the z axis. From top to bottom the values of ε are $10^{-1/2}$, 10^{-1} and $10^{-3/2}$. The crosses show the location of the successive initial conditions for the periodic solutions, corresponding values of z^* are plotted on the horizontal axis. On the vertical axis the trace of the monodromy matrix is plotted.

trace of the differential of $\mathcal{A}$ one obtains the estimate $\sim \varepsilon^{-1/2}$.

6.6 Stable periodic orbits

We keep in mind that the orbits found in subsection 6.5 are hyperbolic and, hence, they can be continued to nearby values of ε. To find stable islands we should find bifurcations of elliptic–hyperbolic points. That is, we should look for the rise of orbits not existing for values of ε larger (or smaller) than some critical value ε_b.

In what follows, we describe a construction showing that stable periodic orbits (of period 1) crossing $\mathcal{D}_1$ and $\mathcal{D}_2$ at $x = 0$ exist at values of ε smaller than any given ε_0. Consider a range $(\varepsilon_{k+1}, \varepsilon_k), \varepsilon_k < \varepsilon_0$ (see the end of Section 2.2). Note that $\varepsilon_k - \varepsilon_{k+1} \sim \varepsilon_k^2$ if we accept that formula (4) describes correctly the splitting. Take a short segment σ of the line $y = z = 0$. Let the middle point M of σ be the closest one to $W^s_{C_2}$ (and, hence, to $W^u_{C_1}$). The distance between the point M and the manifold is of order $\exp(-a_1/\varepsilon)$ (see Section 2.2).

Under the flow of system (1) the image of σ rotates around $W^s_{C_2}$, approaches the surface of the sphere and bends into a parabola-like shape with a tip being the image of M. Under a suitable power N_P of the Poincaré map the image of this point lands on the wedge $\mathcal{D}_2$. At this moment it is at a distance of order one from the saddle-focus C_2.

A simple analysis in the linear approximation shows that it takes a time of order ε^{-2} for the image of M to reach $\mathcal{D}_2$. At this moment the image of σ under the flow of (1) is at a distance of order $\exp(-2a_1/\varepsilon)$ from the surface of the sphere. It implies that the image of a small (in fact, exponentially small) vicinity of M on σ under N_P iterations of the Poincaré map lies in $\mathcal{D}_2$ at a distance of order $\exp(-2a_1/\varepsilon)$ from its border N_2S_2 (see figure 1 (b)). Denoting the distance between the tip of this image and C_2 as r_f, one finds in the linear approximation $\mathrm{d}r_f/\mathrm{d}\varepsilon \sim \varepsilon^{-2}$. Hence, at different values of ε we find the image of M in $\mathcal{D}_2$ at different positions with respect to the z-axis. It is important to note that it traverses $\mathcal{D}_2$ many times while the value of ε varies from ε_{k+1} and ε_k. A priori we cannot say if it travels from $x > 0$ to $x < 0$ or vice versa, because the position of the intersection of $W^s_{C_2}$ with $z = 0$ occurs for values $y = y^*(\varepsilon)$, which change sign as mentioned in section 2.2 (see figure 2 (b)).

Assume that at $\varepsilon = \varepsilon_*$ the image of this small vicinity of M is tangent to the z-axis. At this value of ε two periodic orbits are born, one stable and the other unstable. The stable one exists in some range of ε larger (or smaller, depending on the sign of y^*) than ε_*. The island of stability surrounding this orbit in $\mathcal{D}_1$ lies in a band of width of order $\exp(-2a_1/\varepsilon)$ and, thus, it is exponentially small.

Recall (see Section 2.2) that $a_1 \approx 12$. This is the reason why we succeeded in finding the islands numerically only at sufficiently large values of ε.

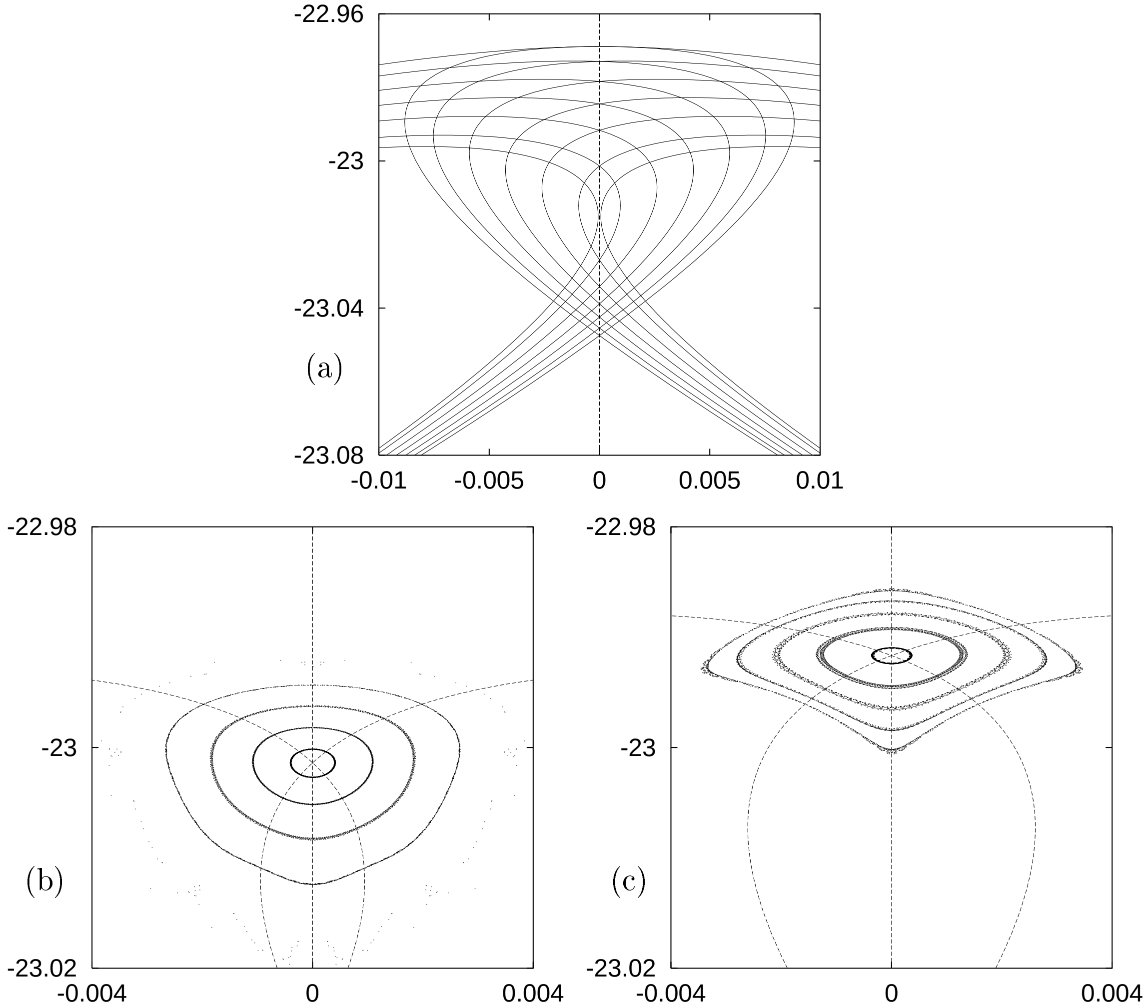

Figure 20: (a) Images of suitable pieces of the line $y = z = 0$ until they enter $\mathcal{D}_2$ for different values of ε. (b) and (c) show stable islands for $\varepsilon = 1.03595$ and 1.03590, respectively. On the horizontal axis the value of x is plotted. On the vertical one the variable is $\log(1 - (x^2 + z^2)^{1/2})$.

To select suitable values of ε and an initial segment on $y = z = 0$ we make, first, the following considerations:

- The value of ε cannot be much larger than 1, as mentioned in section 2.2, because then the lines ON_j, ON_j, $j = 1, 2$ are not defined.

- If the distance $|y^*(\varepsilon)|$ from the x axis to the intersection of $W^s_{C_2}$ with the plane $z=0$ is a small quantity, δ, then the tip of the image of the segment when it reaches $\mathcal{D}_2$ is at a distance of the order of δ^2 from the circle boundary. For $\varepsilon = 1$ one has $|y^*(\varepsilon)| = 0.42 \times 10^{-5}$. This, together with the previous consideration, strongly suggests to look for values of ε slightly greater than 1.

- For a given value of ε one should compute the point of intersection of $W^s_{C_2}$ with $z=0$. Let $(x^*(\varepsilon), y^*(\varepsilon))$ be this intersection. Then we scan initial points on $y=z=0$ with x in a range of amplitude 10^{-4} centred at $x^*(\varepsilon)$.

This allows to detect curves like the ones shown in figure 20 (a). The plotted lines are obtained for values of ε equal to 1.03598, 1.03595, 1.03590, 1.03585, 1.03580, 1.03575 and 1.03571. Together with each curve we plot the symmetrical one with respect to the vertical axis. The number of Poincaré iterates to go from $y=z=0$ to $\mathcal{D}_2$ is equal to 9. The vertical variable measures the distance to the boundary in logarithmic scale. The first value of ε is close to a quadratic tangency on $x=0$, when the elliptic–hyperbolic bifurcation is produced. Last one is close to a cubic tangency with the symmetric curve. It corresponds to a period doubling bifurcation. In figure 20 (b) and (c) a couple of representative islands are shown.

Note that the range of values of ε for which this family of islands exist is less than 3×10^{-4}. Furthermore, an island like the one shown in part (b) of the figure has an amplitude 0.006 in x, 2×10^{-12} in z and is located at 10^{-10} from the boundary. A similar bifurcation (requiring 10 Poincaré iterates instead of 9) has been found for ε in the range $[1.013, 1.014]$, but it occurs at 3×10^{-11} from the boundary and it is not shown here. In this decrease of the distance to the boundary not only the fact that ε decreases is relevant. It plays also an important role the oscillating character of $y^*(\varepsilon)$. See figure 2 (b) to check the effect of the sinusoidal term around these values of ε. Some zeros of $y^*(\varepsilon)$ occur near 1.31042, 0.97090, 0.77355, 0.64383, 0.55179, $\ldots$. Going from 1.036 to 1.013 we are approaching one of these zeros. A rough estimate of the distance of these "simplest" islands to the boundary is $O(\exp(-24/\varepsilon))$.

Figure 21 shows one of the elliptic periodic orbits found in this way. Note that it closes after one turn around the y axis. It is easy to show (but not so easy to compute!) the existence of periodic orbits closing after several turns around the y axis.

In fact one can strongly suspect that the islands, despite they are extremely small, must be present for a dense set of values of ε. Indeed, a tip of the image of $y=z=0$, like the ones shown in figure 20 (a), but not giving rise to an island directly in $\mathcal{D}_2$, must appear, under successive iterates of the return map, at almost any place in the wedge. Furthermore it should travel very quickly when moving ε, specially after a large number of iterates. This network of extremely narrow "fingers" should intersect the symmetric ones (or the symmetric of the ones obtained using a different number of iterates) at values of ε as close as desired.

Conclusions

Despite the system studied is a small perturbation of an integrable flow in the 3D ball, it seems to display a chaotic behaviour, for arbitrarily small perturbations, in most of the phase space. The numerically found statistical properties of the system are quite

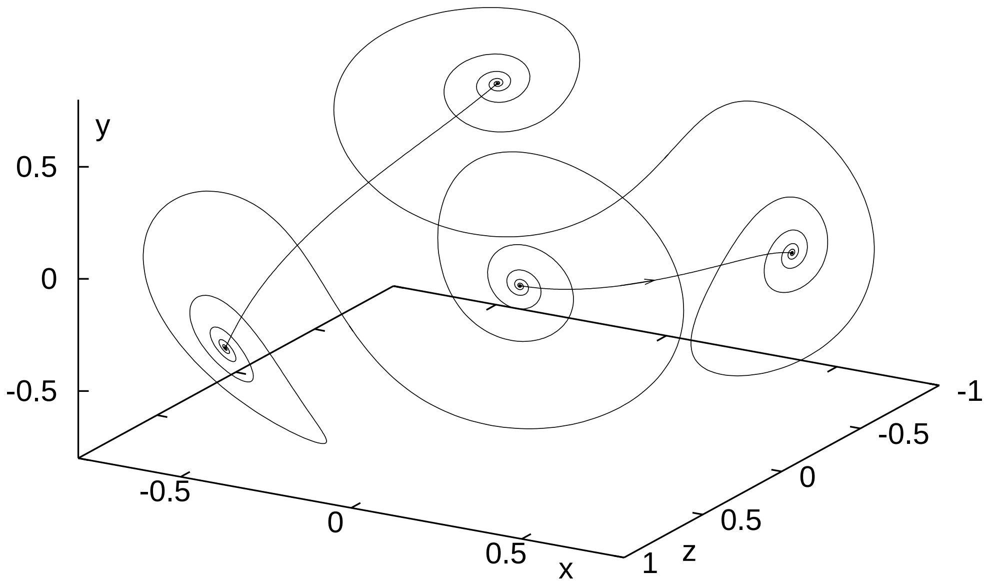

Figure 21: A 3D view of a stable periodic orbit for $\varepsilon = 1.03574$. Initial conditions $x = 0.5116638091963109$, $y = z = 0$. Period $= 62.765832$.

indistinguishable from those of an ergodic system. These properties are in good agreement with analytical results obtained using the theory of adiabatic invariants and their changes at a separatrix. Geometrical properties of the system suggest hyperbolicity on a large part of the domain of definition of the corresponding return map. This is also supported by the numerics. On the other hand, the geometry of the invariant manifolds (in particular, exponentially small splitting of the 1-dimensional manifolds) produces stable periodic solutions, surrounded by stability islands (invariant tori). However, the impact of these islands on the statistics is absolutely negligible, because their measure is exponentially small with the perturbation parameter. The system can be considered ergodic for any practical purpose. The analytic and numeric tools used to justify this assertion can be used for other systems to check the ranges of parameters for which they can be accepted as ergodic (eventually with a prescribed tolerance).

Acknowledgements

The authors acknowledge the support of INTAS grant No. 00-221. The first and third authors acknowledge support of RFBR grant No. 00-01-00538. They thank the second author and the Departament de Matemàtica Aplicada i Anàlisi of the University of Barcelona for hospitality. The research of the second author has been partly supported by grants BFM2000-805 (Spain) and 2000SGR-27/2001SGR-70 (Catalonia). The computing facilities of the UB-UPC Group of Dynamical Systems have been used.

A Appendix. Proofs and computation details.

A.1 Exponentially small splitting of the 1D manifolds $W^{u,s}_{C_j}$

In the unperturbed problem ($\varepsilon = 0$) there exists an ellipse $\mathcal{E}$ of degenerate elliptic fixed points (see Section 2.1). Under the perturbation this ellipse is destroyed, and (weakly) hyperbolic fixed points C_j together with their invariant manifolds appear in its small vicinity. In this appendix we show that the distance between the points of the first intersection of the manifold whiskers $W^u_{C_1}$ and $W^s_{C_2}$ with the plane $z = 0$ (inside the unit sphere) is exponentially small (i.e. $\mathrm{O}(\exp(-\mathrm{const}/\varepsilon))$. Then, this is obviously valid also for $W^u_{C_3}$ and $W^s_{C_4}$.

Let $\mathcal{E}_1$ be the part of $\mathcal{E}$ that is inside the unit sphere at $x > 0$. Introduce in a vicinity of $\mathcal{E}_1$ new coordinates l, ξ_1, ξ_2 in such a way that the unperturbed system in these coordinates has the form

$$\begin{aligned} \dot{\boldsymbol{\xi}} &= \mathrm{A}(l)\boldsymbol{\xi} + \mathrm{O}(|\boldsymbol{\xi}|^2), \qquad \boldsymbol{\xi} = (\xi_1, \xi_2), \\ \dot{l} &= 0, \end{aligned} \tag{38}$$

and $\mathrm{A}(l)$ is a non-degenerate matrix. Here l is a value of the integral L (see (3)) at a point (x, y, z). Note, that at the endpoints of $\mathcal{E}_1$ we have $l = \pm 2/5^{5/8}$. We recall that, according to Section 2.2, the eigenvalues of $\mathrm{A}(l)$ are purely imaginary and bounded away from zero from C_1 to C_2. Variables ξ_1, ξ_2 can be defined, for instance, as follows. Consider the surface $L = l$ passing through the point (x, y, z). It crosses $\mathcal{E}_1$ at a point $(x_1, 0, z_1)$. Consider the plane Π tangent to the surface $L = l$ at this point. In this plane, we introduce Cartesian coordinates with one axis belonging to the plane $y = 0$ and the other orthogonal to this plane. Then ξ_1, ξ_2 are coordinates in this coordinate system of the orthogonal projection of (x, y, z) onto Π.

In variables l, ξ_1, ξ_2 the equations of the perturbed motion take the form

$$\begin{aligned} \dot{\boldsymbol{\xi}} &= \mathrm{A}(l)\boldsymbol{\xi} + f(l, \boldsymbol{\xi}) + \varepsilon h(l, \boldsymbol{\xi}, \varepsilon), \\ \dot{l} &= \varepsilon g(l, \boldsymbol{\xi}, \varepsilon), \end{aligned} \tag{39}$$

where A, f, g, h are analytic functions of their arguments, $f = \mathrm{O}(|\boldsymbol{\xi}|^2)$, $g(\pm 2/5^{5/8}, 0, 0) = 0$. According to [15], there exists an analytic change of variables $\boldsymbol{\xi} = \bar{\boldsymbol{\xi}} + \mathrm{O}(\varepsilon)$ such that

$$\begin{aligned} \dot{\bar{\boldsymbol{\xi}}} &= \bar{\mathrm{A}}(l)\bar{\boldsymbol{\xi}} + \mathrm{O}(|\bar{\boldsymbol{\xi}}|^2) + \mathrm{O}(\exp(-\mathrm{const}/\varepsilon)), \\ \dot{l} &= \varepsilon \bar{g}(l, \bar{\boldsymbol{\xi}}, \varepsilon). \end{aligned} \tag{40}$$

Omitting exponentially small terms we obtain a system with fixed points $\bar{\mathrm{C}}_{1,2} = (\pm 2/5^{5/8}, 0, 0) + \mathrm{O}(\varepsilon)$. The unstable whisker of $\bar{\mathrm{C}}_1$ coincides with the stable whisker of $\bar{\mathrm{C}}_2$: both whiskers are defined by $\bar{\xi}_1 = \bar{\xi}_2 = 0$. The influence of the omitted exponentially small term can result in only exponentially small splitting of these whiskers. Therefore, in the original coordinates, the distance between the points of the first intersection of the unstable whisker of C_1 and the stable whisker of C_2 with the plane $z = 0$ is also exponentially small.

A.2 Proof of formulae (5)

A point inside of the unit sphere that does not belong to the separatrix, nor to the plane $z = 0$, can be specified by the coordinates i, j, ϕ where i, j are the values of I, J at the point, and ϕ mod2π is an angle variable on the phase trajectory passing through the point. In terms of these variables, the system (1) has the following form:

$$\begin{aligned}
\frac{\mathrm{d}i}{\mathrm{d}t} &= \varepsilon f(i,j,\phi),\\
\frac{\mathrm{d}j}{\mathrm{d}t} &= \varepsilon g(i,j,\phi),\\
\frac{\mathrm{d}\phi}{\mathrm{d}t} &= \omega(i,j) + \varepsilon h(i,j,\phi).
\end{aligned}$$

Here functions f, g, h are 2π-periodic in ϕ. Define the averaged system:

$$\frac{\mathrm{d}i}{\mathrm{d}t} = \varepsilon F(i,j), \qquad \frac{\mathrm{d}j}{\mathrm{d}t} = \varepsilon G(i,j), \tag{41}$$

where F and G are the averages of f and g over ϕ. It follows from this definition that

$$\begin{aligned}
F(i,j) &= \frac{1}{T(i,j)} \oint (\mathrm{grad}\, I, \mathbf{w})\mathrm{d}t,\\
G(i,j) &= \frac{1}{T(i,j)} \oint (\mathrm{grad}\, J, \mathbf{w})\mathrm{d}t,
\end{aligned} \tag{42}$$

where the integrals are evaluated along the phase trajectory of the unperturbed system with $I = i$, $J = j$, and T is the period on this phase trajectory.

Consider now the quantity $\Delta\Phi = \Phi(i + \Delta i, j) - \Phi(i, j)$ at $i > 0, j > 0$. We have

$$\Delta\Phi = -\int_{\Delta\Sigma} (\mathbf{w}, \mathbf{n})\mathrm{d}\sigma, \tag{43}$$

where $\Delta\Sigma$ is the part of the surface $\{J = j\}$ bounded by the unperturbed phase trajectories $\{I = i, J = j\}$ and $\{I = i + \Delta i, J = j\}$, $\mathrm{d}\sigma$ and $\mathbf{n}$ are an area element on Σ and a unit normal vector on it, directed as described in subsection 2.2. The minus sign in (43) is due to the fact that the area bounded by the curve $\{I = i, J = j\}$ on the surface $\{J = j\}$ contracts as i increases.

Introduce the tangential vector $\mathrm{d}\mathbf{l}$ on the unperturbed phase trajectory $\{I = i, J = j\}$:

$$\mathrm{d}\mathbf{l} = [\mathrm{grad}\, I, \mathrm{grad}\, J]\mathrm{d}t, \tag{44}$$

where $[\cdot,\cdot]$ is a vector product, and $\mathrm{d}t$ is a time element in motion along the trajectory. Next, introduce the following vector on the curve $\{I = i, J = j\}$:

$$\Delta\mathbf{r} = \frac{[\mathrm{grad}\, J, \zeta]\Delta i}{(\mathrm{grad}\, I, \mathrm{grad}\, J, \zeta)}, \tag{45}$$

where ζ is an arbitrary vector non coplanar with $\mathrm{grad}\, I, \mathrm{grad}\, J$, and $(\cdot,\cdot,\cdot)$ is a mixed product. The vector $\Delta\mathbf{r}$ is orthogonal to $\mathrm{grad}\, I$ and $\mathrm{grad}\, J$ and its end point lies on the curve $\{I = i + \Delta i, J = j\}$ to within $\mathrm{O}(\Delta i^2)$ since $(\mathrm{grad}\, I, \Delta\mathbf{r}) = \Delta i$. Thus, using (43)-(45), we find in the main approximation in Δi:

$$\Delta\Phi = \oint (\mathbf{w}, [\Delta\mathbf{r}, \mathrm{d}\mathbf{l}]) = -\oint (\mathbf{w}, \mathrm{grad}\, J)\Delta i\, \mathrm{d}t. \tag{46}$$

From (41), (42), and (46) in the limit as $\Delta i \to 0$, one obtains the second formula in (5). This formula in the case $i < 0$ and the first formula can be proved similarly.

A.3 Asymptotic expansion of Φ near the separatrix

In this subsection, we prove formulae (7) and (9).

Introduce the vector potential of the perturbation $\mathbf{A}$: $\mathrm{rot}\mathbf{A} = \mathbf{w}$, $\mathbf{A} = -\frac{1}{2}(0, x^2+z^2, 0)$. From (6), one finds the following formula for the adiabatic invariant Φ:

$$\Phi(i,j) = \oint_{\partial\Sigma} (\mathbf{A}, \mathrm{d}\mathbf{l}) = -\frac{1}{2} j \oint_{\partial\Sigma} z^3 \mathrm{d}y, \tag{47}$$

where $\mathrm{d}\mathbf{l} = (\mathrm{d}x, \mathrm{d}y, \mathrm{d}z)$, and $\partial\Sigma$ is the boundary of the surface Σ, i.e. the unperturbed phase trajectory $\{I = i, J = j\}$. Let $|i| \ll 1$, and consider for definiteness the case $i > 0$. Then we have

$$\Phi(i,j) = -\frac{1}{2} j \oint_{\Gamma_{i,j}} z^3 \mathrm{d}y, \qquad \Phi_0(j) = -\frac{1}{2} j \int_{s_j} z^3 \mathrm{d}y. \tag{48}$$

Choose a certain small $\delta, 0 < \delta < 1$ and consider the planes $y = 1 - \delta$ and $y = -1 + \delta$. For sufficiently small i, they cut the contour $\Gamma_{i,j}$ and divide it into four parts (see figure 4): segment BC near the plane $x = 0$, segment DA near the plane $z = 0$, and segments AB and CD near the poles of the sphere. Similarly, the contour $\Gamma^+_{0,j}$ is divided into four segments by the points A_0, B_0, C_0, and D_0. According to (2), we have along $\Gamma_{i,j}$

$$i = xz^4, \; jz^3 = x^2 + y^2 + z^2 - 1. \tag{49}$$

Hence we find that on BC

$$y^2 = jz^3 - z^2 + 1 + \mathrm{O}_\delta(i^2).$$

The subscript δ denotes that the estimate is not, generally, uniform in δ. The part of $\Phi(i,j)$ associated with the segment BC is

$$\Phi^{BC}(i,j) = -\frac{1}{2} j \int_{BC} z^3 \mathrm{d}y = -\frac{1}{2} j \int_{B_0C_0} z^3 \mathrm{d}y + \mathrm{O}_\delta(i^2) = \Phi_0(j) + f_1(\delta) + \mathrm{O}_\delta(i^2),$$

where $f_1(\delta) = \mathrm{O}(\delta^{5/2})$. Note that function $f_1(\delta)$ and all functions f_k below do not depend on i.

On the segment DA

$$x = \sqrt{1-y^2} + \mathrm{O}_\delta(i^{1/2}).$$

Hence,

$$\begin{aligned}
\Phi^{DA}(i,j) &= -\frac{1}{2} j \int_{DA} z^3 \mathrm{d}y = \frac{1}{2}|j| \int_{DA} \left(\frac{i}{x}\right)^{3/4} \mathrm{d}y \\
&= \frac{1}{2}|j| i^{3/4} \int_{DA} \frac{\mathrm{d}y}{(1-y^2)^{3/8}} + \mathrm{O}_\delta(i^{5/4}) \\
&= \frac{1}{2}|j| i^{3/4} \int_{-1}^{1} \frac{\mathrm{d}y}{(1-y^2)^{3/8}} + i^{3/4} f_2(\delta) + \mathrm{O}_\delta(i^{5/4}),
\end{aligned}$$

where $f_2(\delta) = \mathrm{O}(\delta^{5/8})$. Evaluating the integral, we obtain

$$\Phi^{DA}(i,j) = |j| i^{3/4} \frac{\sqrt{\pi}}{2} \frac{\Gamma(5/8)}{\Gamma(9/8)} + i^{3/4} f_2(\delta) + \mathrm{O}_\delta(i^{5/4}).$$

When considering the integral on the segment AB, it is convenient to use z as the integration variable:

$$\Phi^{AB}(i,j) = -\frac{1}{2}j\int_{AB} z^3 \mathrm{d}y = -\frac{1}{4}j\int_{z_A}^{z_B} \frac{z^3(3jz^2 - 2z + 8i^2/z^9)}{(1 - z^2 + jz^3 - i^2/z^8)^{1/2}}\mathrm{d}z,$$

where $z_B \sim \sqrt{\delta}$, $z_A \sim i^{1/4}/\delta^{1/8}$. We find:

$$\begin{aligned}\Phi^{AB}(i,j) &= -\frac{1}{4}j\int_0^{z_B} \frac{z^3(3jz^2 - 2z)}{(1 - z^2 + jz^3)^{1/2}}\mathrm{d}z + i^{3/4}\mathrm{O}(\delta^{5/8}) + \mathrm{O}_\delta(i^{5/4}) \\ &= i^{3/4}f_3(\delta) + f_4(\delta) + \mathrm{O}_\delta(i^{5/4}),\end{aligned}$$

where $f_3(\delta) = \mathrm{O}(\delta^{5/8})$, $f_4(\delta) = \mathrm{O}(\delta^{5/2})$.

Combining the above expressions, one obtains:

$$\begin{aligned}\Phi(i,j) &= \Phi_0(j) + f_5(\delta) + i^{3/4}\left(-\frac{4}{3}a|j| + f_6(\delta)\right) + \mathrm{O}_\delta(i^{5/4}), \\ a &= -\frac{3\sqrt{\pi}}{8}\frac{\Gamma(5/8)}{\Gamma(9/8)},\end{aligned} \tag{50}$$

where $f_5(\delta) = \mathrm{O}(\delta^{5/2})$, $f_6(\delta) = \mathrm{O}(\delta^{5/8})$. Since the left-hand side in (51) is independent of δ, we finally find that

$$\Phi(i,j) = \Phi_0(j) - \frac{4}{3}a|j||i|^{3/4} + \mathrm{O}(i^{5/4}). \tag{51}$$

For $\Theta = \partial\Phi_0/\partial j$ one obtains from (8) that

$$\Theta = \int_{s_j} z^5 \mathrm{d}t = \frac{1}{2}\int_{s_j}\frac{z^4}{y}\mathrm{d}z = \int_0^Z \frac{z^4 \mathrm{d}z}{\sqrt{jz^3 - z^2 + 1}},$$

and introducing the integration variable $v = z/Z$, we arrive at (9).

A.4 Change in the adiabatic invariant at a separatrix crossing

In this subsection, formula (10) is derived. For definiteness, we consider the case $i_0 < 0$. The separatrix is crossed in the direction from $i < 0$ to $i > 0$. The accuracy of this formula is estimated in the next subsection.

It can be shown that

(1) the quantity i_0 satisfies the inequalities

$$0 > i_0 > -\varepsilon\Theta_0 - C\varepsilon^{7/4};$$

(2) if

$$-C\varepsilon^{7/4} > i_0 > -\varepsilon\Theta_0 + C\varepsilon^{7/4}, \tag{52}$$

then

$$i_1 = i_0 + \varepsilon\Theta_0 + \mathrm{O}(\varepsilon^{7/4}) > \frac{C}{2}\varepsilon^{7/4}, j_1 = j_0 + \varepsilon\mathrm{O}(i_1^{-1/4}),$$

where C is a positive constant.

The proof is based on the fact that that on the turn γ_0 the value i grows by the amount $\varepsilon\Theta_0 + \mathrm{O}(\varepsilon^{7/4})$ provided that the phase point does not come too close to the saddles at the poles of the sphere. The condition (52) ensures that the trajectory does not approach the poles too closely. It is assumed in derivation of formula (10) that this condition is satisfied.

One has for the time derivatives of I, J along the motion in the exact system:

$$\frac{\mathrm{d}I}{\mathrm{d}t} = \varepsilon(\mathrm{grad}\, I, \mathbf{w}) = \varepsilon z^3(z^2 - 4x^2), \tag{53}$$

$$\frac{\mathrm{d}J}{\mathrm{d}t} = \varepsilon\,(\mathrm{grad}\, J, \mathbf{w}) = \varepsilon x\frac{(x^2+y^2+z^2-1)}{z^4} = \varepsilon J\frac{x}{z}\,. \tag{54}$$

Consider a turn γ_k with small value of i_k (i.e. close to separatrix). It follows from (53) that variation in I along γ_k occurs mainly on that part of turn that lies near the separatrix; the other part of the turn is close to the plane $z = 0$, and $\mathrm{d}I/\mathrm{d}t$ is small here. Similarly, from (54) one can see that the main variation in J along γ_k occurs near the plane $z = 0$. To find the variations in I and J, we have to integrate (53), (54) over time t along γ_k. Replace integration along the turn γ_k by integration along the unperturbed trajectory $\{I = i_k, J = j_{k-1}\}$. These latter integrals can be evaluated either directly, or from the averaged system (5) and the expansion (7). Estimating the errors due to changing the integration contour, we find

$$\begin{aligned} i_k - i_{k-1} &= \delta I_k + \varepsilon^2\mathrm{O}(i_k^{-1/4}) = \varepsilon\Theta(j_{k-1}) + \varepsilon\mathrm{O}\left(i_1^{-1/4}\right) + \varepsilon^2\mathrm{O}(i_k^{-1/4}),\\ j_k - j_{k-1} &= \delta J_k + \varepsilon^2\mathrm{O}(i_k^{-1/2}) = \varepsilon a|j_{k-1}||i_1|^{-1/4}\mathrm{sign}(i_k) + \varepsilon\mathrm{O}(i_k^{-1/4}) + \varepsilon^2\mathrm{O}(i_k^{-1/2}), \end{aligned} \tag{55}$$

where

$$\delta I_k = \varepsilon\frac{\partial\Phi(i_k, j_{k-1})}{\partial j}, \quad \delta J_k = -\varepsilon\frac{\partial\Phi(i_k, j_{k-1})}{\partial i}. \tag{56}$$

For the function $\Phi(i,j)$ on γ_k one finds from (7) that

$$\Phi\,(i,j) = \Phi_0(j_0) + \Theta_0(j-j_0) - \frac{4}{3}a|j_0||i|^{3/4} + \mathrm{O}(|i|^{5/4} + |j-j_0|^2 + |j-j_0||i|^{3/4}). \tag{57}$$

From (55), (57) it follows that

$$\begin{aligned} \Phi_k - \Phi_{k-1} = -a|j_0|\left(-\varepsilon\Theta_0|i_k|^{-1/4}\mathrm{sign}(i_k) + \frac{4}{3}|i_k|^{3/4} - \frac{4}{3}|i_{k-1}|^{3/4}\right)\\ +\mathrm{O}\left(|i_k|^{5/4} + |i_{k-1}|^{5/4} + |j_0 - j_k|^2 + |j_0 - j_{k-1}|^2 + |j_0 - j_k||i_k|^{3/4} + |j_0 - j_{k-1}||i_{k-1}|^{3/4}\right). \end{aligned} \tag{58}$$

The change in Φ on a turn far enough from the separatrix (at a distance ~ 1 from it) is $\mathrm{O}(\varepsilon^2)$ since Φ is an adiabatic invariant. The total change in Φ over such turns is $\mathrm{O}(\varepsilon)$. Therefore, the lower-order in ε term in the asymptotic expression for the total change in Φ is due to the turns near the separatrix. Hence, $\Delta\Phi$ can be calculated in the leading approximation with the use of (55), (58). The final result is as follows (the remainder term is estimated in the following subsection):

$$\Delta\Phi = -a|j_0|\sum_{k=-N+1}^{N}\left[-\varepsilon\Theta_0\frac{\mathrm{sign}(i_0 + k\varepsilon\Theta_0)}{|i_0 + k\varepsilon\Theta_0|^{1/4}} + \frac{4}{3}\left(|i_0 + k\varepsilon\Theta_0|^{3/4} - |i_0 + (k-1)\varepsilon\Theta_0|^{3/4}\right)\right] + \mathrm{O}(\varepsilon), \tag{59}$$

where N is an integer $\sim \varepsilon$ (the leading term in the asymptotics does not depend on the exact choice of N). Substituting $\xi = -i_0/\varepsilon\Theta_0$, one obtains

$$\Delta\Phi = \varepsilon^{3/4} a|j_0|\Theta_0^{3/4} \sum_{k=-N+1}^{N} \frac{\mathrm{sign}(\xi+k)}{|-\xi+k|^{1/4}} + \mathrm{O}(\varepsilon). \tag{60}$$

Using the definition of the gamma function

$$\Gamma\left(\frac{1}{4}\right) = p^{1/4}\int_0^\infty t^{-3/4}\mathrm{e}^{-pt}\mathrm{d}t, \quad p>0,$$

one finds for $\xi > 0$

$$\sum_{n=0}^{N-1} \frac{1}{(\xi+n)^{1/4}} = \frac{1}{\Gamma(1/4)}\sum_{n=0}^{N-1}\int_0^\infty t^{-3/4}\mathrm{e}^{-(\xi+n)t}\mathrm{d}t = \frac{1}{\Gamma(1/4)}\int_0^\infty \frac{t^{-3/4}e^{-\xi t}}{1-\mathrm{e}^{-t}}\left(1-\mathrm{e}^{-Nt}\right)\mathrm{d}t.$$

Substituting this expression in (60), in the limit as $N\to\infty$ we obtain

$$\Delta\Phi = -\varepsilon^{3/4}a|j_0||\Theta_0|^{3/4}\frac{1}{\Gamma(1/4)}\int_0^\infty \frac{t^{-3/4}\left(\mathrm{e}^{-\xi t}-\mathrm{e}^{-(1-\xi)t}\right)}{1-\mathrm{e}^{-t}}\mathrm{d}t + \mathrm{O}(\varepsilon). \tag{61}$$

Changing the integration variable $t\to w^4$ and noting that we can replace in the formula j_0 by j_* without altering the magnitude of the remainder term, we finally arrive at (10).

A.5 On the accuracy of the formula for the change in the adiabatic invariant

Consider the turns γ_k with $k\neq 0,1,2$. On these turns, we have $|i_k| > C_3^{-1}\varepsilon$ where C_3 is a positive constant. Hence, terms of order ε in (55) dominate over terms of order ε^2. One finds from (55) that

$$\begin{aligned} i_k &- i_{k-1} > C_4^{-1}\varepsilon, \quad C_4 = \mathrm{const} > 0, \\ i_k &= i_0 + k\varepsilon\Theta_0 + \mathrm{O}\left(|i_k|^{7/4}\right), \\ j_k &= j_0 + \mathrm{O}\left(|i_k|^{3/4}\right). \end{aligned} \tag{62}$$

From (7), (55), and (56) one obtains the formula for the change in the adiabatic invariant on the turn γ_k:

$$\Delta\Phi_k = \Phi_k - \Phi_{k-1} = \Phi(i_{k-1}+\delta I_k, j_{k-1}+\delta J_k) - \Phi(i_{k-1},j_{k-1}) + \varepsilon^2\mathrm{O}\left(|i_k|^{-1/2}\right) \tag{63}$$

Note that the right-hand side of this expression, if formally expanded into powers of ε, is a quantity of the order of ε^2, as should be the case because of the adiabatic invariance of Φ. We transform (63) with the use of (55) and (56):

$$\begin{aligned}\Delta\Phi_k = \quad & \Phi\left(i_{k-1}+\varepsilon\frac{\partial\Phi(i_k,j_{k-1})}{\partial j}, j_{k-1}\right) - \Phi(i_{k-1},j_{k-1}) - \varepsilon\frac{\partial\Phi(i_k,j_{k-1})}{\partial j}\frac{\partial\Phi(i_k,j_{k-1})}{\partial i} \\ & + \varepsilon^2\mathrm{O}\left(|i_k|^{-1/2}\right).\end{aligned}$$

Replacing j_{k-1} in the right-hand side of this expression with j_0, and estimating the error introduced thereby with the use of (62), we obtain

$$\Delta\Phi_k = \Phi\left(i_{k-1} + \varepsilon\frac{\partial\Phi(i_k, j_0)}{\partial j}, j_0\right) - \Phi\left(i_{k-1}, j_0\right) - \varepsilon\frac{\partial\Phi(i_k, j_0)}{\partial j}\frac{\partial\Phi(i_k, j_0)}{\partial i} + \varepsilon^2\mathrm{O}\left(|i_k|^{-1/2}\right).$$

Introduce Φ_a, Φ_b:

$$\begin{aligned}\Phi &= \Phi_a(i,j) + \Phi_b(i,j),\\ \Phi_a(i,j) &= \Phi_0(j) - \frac{4}{3}a|j||i|^{3/4}.\end{aligned}$$

According to (7), $\Phi_b(i,j) = \mathrm{O}\left(|i|^{5/4}\right)$. In terms of the new notations,

$$\Delta\Phi_k = \Phi_a\left(i_{k-1} + \varepsilon\frac{\partial\Phi(i_k, j_0)}{\partial j}, j_0\right) - \Phi_a\left(i_{k-1}, j_0\right) - \varepsilon\frac{\partial\Phi(i_k, j_0)}{\partial j}\frac{\partial\Phi_a(i_k, j_0)}{\partial i}$$

$$+\Phi_b\left(i_{k-1} + \varepsilon\frac{\partial\Phi(i_k, j_0)}{\partial j}, j_0\right) - \Phi_b(i_{k-1}, j_0) - \varepsilon\frac{\partial\Phi(i_k, j_0)}{\partial j}\frac{\partial\Phi_b(i_k, j_0)}{\partial i} + \varepsilon^2\mathrm{O}\left(|i_k|^{-1/2}\right).$$

The set of terms containing Φ_b explicitly, amounts to $\varepsilon^2\mathrm{O}\left(|i_k|^{-3/4}\right)$. Hence

$$\Delta\Phi_k = \Phi_a\left(i_{k-1} + \varepsilon\frac{\partial\Phi(i_k, j_0)}{\partial j}, j_0\right) - \Phi_a\left(i_{k-1}, j_0\right) - \varepsilon\frac{\partial\Phi(i_k, j_0)}{\partial j}\frac{\partial\Phi_a(i_k, j_0)}{\partial i} + \varepsilon^2\mathrm{O}\left(|i_k|^{-3/4}\right).$$

In the last expression, replace $\partial\Phi(i_k, j_0)/\partial j$ with Θ_0, i_k with $i_{k-1} + \varepsilon\Theta_0$, and i_{k-1} with $i_0 + (k-1)\varepsilon\Theta_0$; this introduces an additional error $\varepsilon^2\mathrm{O}(|i_k|^{-1/2})$. Hence

$$\begin{aligned}\Delta\Phi_k = &- a|j_0|\left[-\varepsilon\Theta_0\frac{\mathrm{sign}\,(i_0 + k\varepsilon\Theta_0)}{|i_0 + k\varepsilon\Theta_0|^{1/4}} + \frac{4}{3}\left(|i_0 + k\varepsilon\Theta_0|^{3/4} - |i_0 + (k-1)\varepsilon\Theta_0|^{3/4}\right)\right]\\ &+ \varepsilon^2\mathrm{O}\left(|i_k|^{-3/4}\right).\end{aligned} \tag{64}$$

Recall that this relation was obtained for $k \neq 0, 1, 2$. For $k \neq 0, 1, 2$, the situation is simpler because we can use the expansions obtained from (7), (52), and (55):

$$\begin{aligned}\Phi(i,j) &= \Phi_0(j_0) + \Theta_0(j - j_0) - \frac{4}{3}a|j_0||i|^{3/4} + \mathrm{O}(\varepsilon),\\ i_k - i_{k-1} &= \varepsilon\Theta_0 + \mathrm{O}(\varepsilon^{25/16}),\\ j_k - j_{k-1} &= -\varepsilon a_0|i_k|^{-1/4}\mathrm{sign}(i_k) + \mathrm{O}(\varepsilon).\end{aligned}$$

Thus we find that the leading term in $\Delta\Phi$ on these turns is the same as in (64), and the error is $\mathrm{O}(\varepsilon)$.

Summing up the above expressions for $\Delta\Phi_k$, and recalling that

$$\varepsilon\sum_{k=-N+1}^{N}|i_k|^{-3/4} = \mathrm{O}(1), \quad k \neq 0, 1, 2,$$

we obtain the estimate given in (61) and (10).

A.6 On the computation of the integral in (19)

To carry out the mentioned integral one should compute, in particular, the averaged flow. To decrease the difficulties due to the presence of unbounded magnitudes, an alternative approach has been used. Let (x^*, z^*) be a point on the plane $y = 0$. For definiteness assume it is inside the domain bounded by the ellipse $\mathcal{E}$. We want to compute the image of this point under the Poincaré map through $y = 0$, $\dot{y} < 0$ in the limit when ε tends to zero. This will allow us to obtain the averaged flow on the (x, z) plane. Let us write

$$x = x_0(t) + \varepsilon x_1(t) + O(\varepsilon^2), \quad y = y_0(t) + \varepsilon y_1(t) + O(\varepsilon^2), \quad z = z_0(t) + \varepsilon z_1(t) + O(\varepsilon^2).$$

Inserting in (1) we obtain the differential equations for x_j, y_j, z_j, $j = 0, 1$. If $j = 0$ they are the equations of the unperturbed problem. For $j = 1$ we have

$$\begin{aligned} \dot{x}_1 &= -8(x_1 y_0 + x_0 y_1) + z_0, \\ \dot{y}_1 &= 22 x_0 x_1 + 6 y_0 y_1 + 2 z_0 z_1, \\ \dot{z}_1 &= 2(y_0 z_1 + y_1 z_0) - x_0. \end{aligned} \tag{65}$$

Equations (65) have to be integrated with zero initial conditions and simultaneously with (1) starting at $(x^*, 0, z^*)$. Let us denote as $v_x(x^*, z^*), v_z(x^*, z^*)$ the final values of x_1, z_1, respectively. Note that due to the fact that the unperturbed vector field on $y = 0$ is orthogonal to this plane, no correction coming from the final value of y_1 has to be applied. Let $T(x^*, z^*)$ be the period of the unperturbed orbit. Furthermore, the value of Ψ can be obtained by integrating $(1 - x_0^2 - y_0^2 - z_0^2)\, \dot{y}_0/2$ along the unperturbed orbit (see formula (48) in this Appendix).

Then the averaged vector field reads

$$\frac{\mathrm{d}x^*}{\mathrm{d}\tau} = v_x(x^*, z^*)/T(x^*, z^*), \quad \frac{\mathrm{d}z^*}{\mathrm{d}\tau} = v_z(x^*, z^*)/T(x^*, z^*). \tag{66}$$

The values of $\Psi(x^*, z^*)$ should remain constant along the averaged path (as it has been checked to occur numerically) and the value of Ω corresponding to this value of Ψ is obtained by integrating $2/T(x^*, z^*)$ from an initial point (x^*, z^*) lying on $x^* = 0$ until it reaches $z^* = 0$.

We should mention how to overcome one difficulty. From (7) it follows that near a point of the form $(0, z_0^*)$ a curve $\Psi = \text{const}$ behaves like $z_0^* - z^* = O((x^*)^{3/4})$. An analysis of the main elements in (66) shows that near $x^* = 0$, $z^* = z_0^*$ we have the following dominant behaviour: $v_x = c_1(z_0^*)$, $v_z = -c_2(z_0^*)(x^*)^{-1/4}$, $T = c_3(z_0^*) - \frac{1}{4}\log(x^*)$, where c_j are functions depending on z_0^*. In particular, the function c_1 is essentially linear in z_0^* for small values of z_0^*. Hence, the vector field in (66) becomes unbounded when $x^* \to 0$. But the main contribution to the value of Ω coming from the part of the path going from $(0, z_0^*)$ to some (x_1^*, z_1^*) with x_1^* small, can be estimated as $2x_1^*/c_1(z_0^*)$. This suggests to start the computation at a point of the form (x_1^*, z_1^*) with $x_1^* = \delta z_1^*$ and δ small. This ensures a uniform bound $O(\delta)$ in the estimate of Ω. The value $\delta = 10^{-7}$ has been selected to produce figure 6.

References

[1] Bajer K and Moffatt H K 1990 On a class of steady confined Stokes flows with chaotic streamlines *J. Fluid Mech.* **212** 337-363

[2] Aref H 1984 Stirring by chaotic advection *J. Fluid Mech.* **143** 1-21

[3] Vainshtein S I and Zel'dovich Ya B 1972 Origin of magnetic fields in astrophysics *Sov. Phys. Usp.* **15** 159-172

[4] Zel'dovich Ya B , Ruzmaikin A A and Sokolov D D 1983 Magnetic fields in astrophysics (Gordon & Breach)

[5] Neishtadt A I and Vasiliev A A 1999 Change of adiabatic invariant at a separatrix in a volume-preserving 3-D system *Nonlinearity* **12** 303-320

[6] Timofeev A V 1978 On the constancy of an adiabatic invariant when the nature of the motion changes *Sov. Phys. JETP* **48** 656-659

[7] Cary J R , Escande D F and Tennyson J 1986 Adiabatic invariant change due to separatrix crossing *Phys. Rev.* **A34** 4256-4275

[8] Neishtadt A I 1986 Change of an adiabatic invariant at a separatrix *Sov.J.Plasma Phys.* **12** 568-573

[9] Neishtadt A I 1987 On the change in the adiabatic invariant on crossing a separatrix in systems with two degrees of freedom *PMM USSR* **51** 586-592

[10] Vainshtein D L , Vasiliev A A and Neishtadt A I 1996 Changes in the adiabatic invariant and streamline chaos in confined incompressible Stokes flow *Chaos* **6** 67-77

[11] Neishtadt A I , Vainshtein D L and Vasiliev A A 1998 Chaotic advection in a cubic Stokes flow *Physica D* **111** 227-242

[12] Neishtadt A I , Sidorenko V V and Treschev D V 1997 Stable periodic motions in the problem of passage through a separatrix *Chaos* **7** 2-11

[13] Bogolyubov N N and Mitropolsky Yu A 1961 *Asymptotic Methods in the Theory of Nonlinear Oscillations* (New York: Gordon and Breach Science Publ. **537**)

[14] Arnold V I , Kozlov V V and Neishtadt A I 1988 *Mathematical aspects of classical and celestial mechanics (Encyclopaedia of mathematical sciences 3)* (Berlin: Springer)

[15] Neishtadt A I 1987 Persistence of stability loss for dynamical bifurcations I *Differential equations* **23** 12 1385-1390